frontiers | Frontiers in Detector Science and Technology

TYPE Original Research
PUBLISHED 07 July 2025
DOI 10.3389/fdest.2025.1585561

OPEN ACCESS

EDITED BY
Armando Francesco Borghesani,
University of Padua, Italy

REVIEWED BY
Marco Guarise,
University of Ferrara, Italy
Ben Jones,
University of Texas at Arlington, United States

*CORRESPONDENCE
R. E. Boltnev,
boltnev@gmail.com

RECEIVED 28 February 2025
ACCEPTED 17 June 2025
PUBLISHED 07 July 2025

CITATION
Boltnev RE and Khmelenko VV (2025) Superfluid helium-4 in porous structures of neon-nitrogen nanoclusters as a target for low-mass dark matter detector.
Front. Detect. Sci. Technol. 3:1585561.
doi: 10.3389/fdest.2025.1585561

Superfluid helium-4 in porous structures of neon-nitrogen nanoclusters as a target for low-mass dark matter detector

R. E. Boltnev[1]* and V. V. Khmelenko[2]

[1]Laboratory of Active Coulomb Systems, Joint Institute for High Temperatures, Russian Academy of Sciences, Moscow, Russia, [2]Department of Physics and Astronomy, Institute for Quantum Science and Engineering, Texas A&M University, College Station, TX, United States

A new concept of three-phase projection chamber filled with a collection of neon-nitrogen nanoclusters immersed in superfluid helium-4 is proposed for detection light dark matter particles with low masses (0.1–10 Gev/c^2). Such a time projection chamber includes a drift region within aerogel-like structure formed by neon-nitrogen nanoclusters filled by superfluid helium and a gas phase camera where electroluminescence takes place. The proposed concept combines the promising properties of liquid helium as a target material for direct detection of light dark matter particles such as high quenching factor, substantial scintillation light, high radiopurity, and high impedance to external vibration noise with the new ones determined by the properties of solid neon and nitrogen. The presence of highly porous impurity structure will enhance the primary scintillation signal (S1) due to light emission stimulated by interactions of metastable He_2 ($a^3\Sigma_u$) molecules and He^+ ions with impurity nanoclusters. The signal of electrons produced by the recoil event (S2) and drifting in external electric field will get additional input due to energy stored in nitrogen atoms stabilized on the nanoclusters' surface.

KEYWORDS

dark matter detection, time projection chamber (TPC), superfluid helium, nanoclusters, rare event searches

1 Introduction

Many astronomical and cosmological observations point to the existence of non-luminous dark matter (DM). So far, DM was revealed exclusively due to its gravitational effects and its nature still remains a puzzle for modern fundamental physics. Theoretical physics suggests many different kinds of particles which can constitute DM (Bertone et al., 2005; Feng, 2010; Baer et al., 2015; Lin, 2019). Expected DM particle mass range spans approximately 50 orders of magnitude - from values ~10^{-22} eV/c^2, for bosons with the de Broglie wavelength ~ 10^{19} m, up to 10^{26} eV/c^2. Direct detection of DM is a great challenge for experimental and theoretical physics–now tens of large scientific collaborations are involved in this activity. So-called weakly interacting massive particles (WIMPs) with a mass in the range $10^9 \div 10^{14}$ eV/c^2 gained a strong experimental interest over the last decades because their detection rates fall into the sensitivity range of elaborated or projected detectors (Lin, 2019). Nevertheless, exclusion limits from both direct detection experiments (Aprile et al., 2023; Aalbers et al., 2023a) and the Large Hadron Collider (ATLAS and CMS collaborations, 2022; ATLAS and CMS collaborations, 2025) stimulate to pay more

attention to light DM particles with masses less than 1 GeV/c^2 (Kahn and Lin, 2022). Light DM particles possess less available kinetic energy, thus detection of their interaction with ordinary matter requires new target materials to achieve much better kinematic matching between DM and the target comparing to that of liquid argon and xenon. Liquid helium (LHe) with its low atomic mass provides rather efficient transfer of kinetic energy from light DM particles. DM particles with a mass range (0.01÷10 GeV/c^2) will interact with a single He atom, triggering an atomic cascade, which eventually includes emission and thermalization of quasi-particles. In the mass range ~0.1 GeV, the helium nuclear recoil energy is still larger than 100 eV, which is sufficient to excite or ionize a helium atom. Then, in superfluid helium-4 (He-II), the recoil energy can dissipate in the following channels (Guo and McKinsey, 2013; You et al., 2023): ionization and conversion of ionized He atoms into excited ones; radiative relaxation of directly excited and neutralized atoms, and highly excited He_2^* excimers; emission of $He_2^*(A^1\Sigma_u^+)$ excimers and formation of metastable $He_2^*(a^3\Sigma_u^+)$; as well as quasi-particle (phonon and roton) excitation. The distribution of the recoil energy via nuclear and electron recoils (NR and ER, respectively) among these interaction channels has been studied experimentally and theoretically (Guo and McKinsey, 2013; Adams et al., 1995; Ito and Seidel, 2013; Hertel et al., 2019; Biekert et al., 2022; Moroshkin et al., 2011). Superfluid helium-4 due to its unique properties provides many different ways to detect light DM particles: the field ionization detection of helium atoms evaporated from surfaces at low temperatures due to energy released upon DM-target interaction (Maris et al., 2017); detection of quasi-particle flux with force-sensitive devices - nanoelectro-mechanical oscillators (You et al., 2023); detection of kinetic excitations of He-II (rotons and phonons) using quantum evaporation and subsequent atomic adsorption onto a calorimeter suspended above the superfluid target (Hertel et al., 2019); conversion of phonons (with energy ~ meV) deposited by scattering process to photons (with energy ~ meV) via optomechanical interaction with a pump laser (Baker et al., 2024); application of magnetic micro-calorimeters for detection phonons in bulk He-II and evaporated atoms in vacuum, heat releases due to absorption of UV photons and quenching metastable He_2^* excimers (von Krosigk et al., 2023). These proposed approaches, based on the unique properties of superfluid helium, along with the exceptionally sensitive germanium detectors (Bhattarai et al., 2023; Acharya et al., 2024) are the most promising for detection of DM particles lighter than MeV/c^2. The new concept of a time projection chamber (TPC) for detection of the charge, scintillation, and triplet helium molecule signals produced by recoil He ions in liquid helium-4 (Guo and McKinsey, 2013) has been elaborated and developed in the project ALETHEIA (Liao et al., 2022; Liao et al., 2023a). ALETHEIA is the first DM direct detection project claiming search DM using the "ER excess only", the "NR excess only", and the "ER and NR excesses combined" channels (Liao et al., 2023b). The current lowest experimental limit for WIMP–nucleon interaction with the spin-independent framework in the high-mass WIMPs region is close to 10^{-47} cm^2 for ≈36 GeV/c^2 WIMPs (Aalbers et al., 2023b). This value is roughly 8 and 1 orders lower than the interaction hypothetically mediated through the Z and the Higgs bosons, ~ 10^{-39} cm^2 and ~ 10^{-46} cm^2, respectively. From this point of view, significantly broader space remains to be explored in the low-mass region: for example, the current limits for WIMPs with mass less than 2 GeV/c^2 are ~ 10^{-38} cm^2, which are one and six orders higher than the interaction mediated by the Z and Higgs boson, respectively. It was estimated that the sensitivity of the ALETHEIA with the exposures of 100 kg*yr and 1 ton*yr will allow to reach the experimental limits ~ 10^{-43} cm^2 and ~ 10^{-44} cm^2, respectively, for WIMPs within the mass range 0.8÷10 GeV/c^2 (Liao et al., 2022).

Here we propose new concept of a three-phase time projection chamber (3P-TPC) for detection of light DM particles with low masses (0.1÷10 GeV/c^2). Such a TPC will consist of a drift region filled by superfluid helium in porous solid structure formed by neon-nitrogen nanoclusters and a gas phase camera for detection of electroluminescence. Liquid helium and solid neon irradiated by high energy particles scintillate brightly in the extreme ultraviolet (EUV) range corresponding to the wavelengths from 10 to 121 nm. Usually, a key aspect of two-phase detectors is the direct optical detection of S1 signal and S2 via secondary scintillation (proportional electroluminescence, for example). S1 and S2 provide a selection of nuclear recoil events caused by elastic collisions with DM. Neon nanoclusters with the characteristic size of 6 nm form very homogeneous transparent aerogel-like (with a wide distribution of the open pore sizes from 8 up to 320 nm) medium within bulk He-II (Kiselev et al., 2001). The densities of helium and neon are ≈2.2·10^{22} and ≈5·10^{20} atoms per cm^3, respectively (Kiryukhin et al., 2007).

The first promising feature of the porous impurity structure is involving of the fraction of the positive ions generated during the recoil event and extracted from recombination area into the S1 signal through radiative relaxation of neutralized atoms produced due to charge transfer from impurity atoms of the nanoclusters. More additional counts to the S1 signal will be provided by the energy transfer from metastable He_2 ($a^3\Sigma_u^+$) molecules to neon/nitrogen atoms of nanoclusters (the diffusion time of the molecule to the cluster's surface is of order 1 μs for the displacement comparable with the maximal pore size): the energy of these molecules will be transferred to the clusters (Jortner et al., 1964) and converted in photons at the time scale ~10^{-6} s instead of long decay of He_2 ($a^3\Sigma_u^+$) molecules with the lifetime of 13 s (McKinsey et al., 1999). Moreover, nitrogen atoms stabilized in neon-nitrogen nanoclusters can also give additional gain to the S2 signal via emission of N_2 ($A^3\Sigma_u^+$) molecules produced due to nitrogen atoms recombination activated by either quantum vortices or electron bubbles drifting through the detector target medium. Therefore, the higher intensity of both S1 and S2 signals is expected in the proposed three-phase TPC in comparison with a pure LHe TPC.

2 Pure superfluid helium-4 and impurity-helium condensates as target materials for direct DM detection

2.1 Pure He-II

Since helium is the lightest noble element, the same kinetic energy of incident WIMPs would result in larger recoil energy than other elements, excluding hydrogen. Next advantage of LHe (including He-II) is its high quenching factor (QF) - a critical

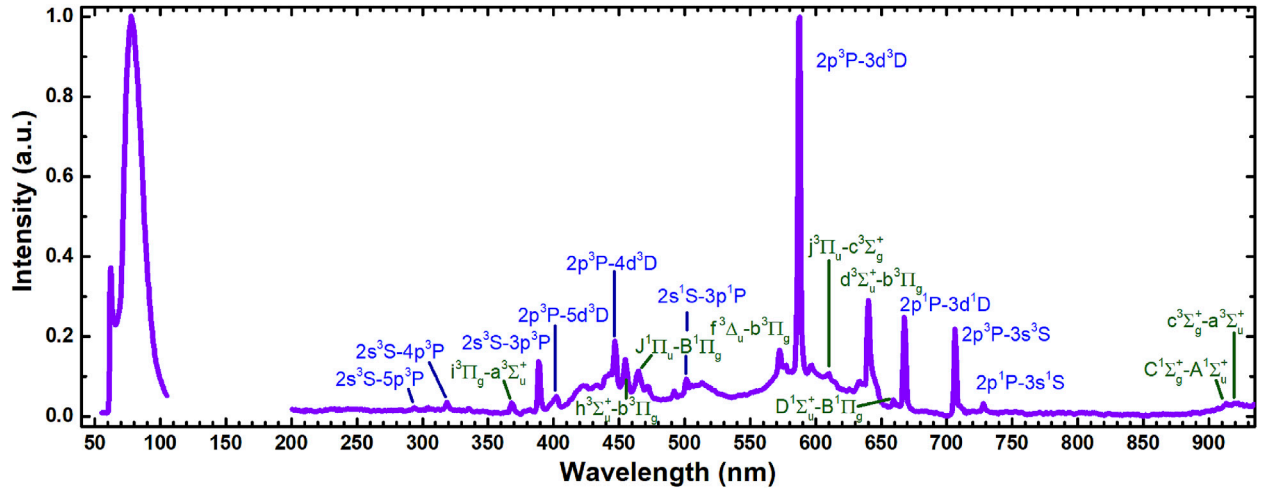

FIGURE 1
Compilation of luminescence spectra of superfluid helium excited by β-particles - EUV range (Surko et al., 1970), and laser irradiation - UV-NIR range (Boltnev et al., 2023). The relative intensities of spectra depend on the excitation method and conditions and may be rather different. Transition assignments of the most intense atomic lines and molecular bands of helium are shown, respectively, by blue and green notes.

parameter for understanding dark matter interactions with nuclei. The quenching factor represents the ratio of ionization and scintillation light yields produced by nuclear recoil to the total energy dissipated in a medium. The data on QF for helium are very scarce. We have found one experimental work with experimental results for IQF (ionization quenching factor - the fraction of energy released by a recoil in a medium through ionization compared with total recoil energy) of helium gas (Santos et al., 2008). The measured IQF of helium is ≈65% for 16 keV nuclear recoil energy, while the IQF of LAr is ≈25% (Cao et al., 2015).

Moreover, superfluid helium-4 possesses some other promising properties as target material for direct detection of light DM particles: different observable and distinguishable signal channels in addition to the total recoil energy, including phonons and rotons (commonly referred as “quasiparticles”), substantial singlet scintillation light, and triplet helium excimers.

In addition, liquid helium is the cleanest fluid - at 4.2 K temperature, ^{3}He and H_2 are the only solvable materials in LHe: the ratios of ^{3}He and H_2 to ^{4}He are $1/(5{\cdot}10^6)$ and $1/10^{10}$ (Abrikosova and Shal’nikov, 1971; Jewell and McClintock, 1979; Gabal et al., 2018), respectively, but at 1.5 K the relative content of H_2 in liquid helium becomes negligible, ~10^{-27}. The ^{3}He and H_2 contents in He-II may be significantly decreased by using microporous filters (Abrikosova and Shal’nikov, 1971; Nakai et al., 1996). The combination of the purity of liquid helium along with its high radiopurity (helium has no long-lived isotopes) provides a material for the DM detector target with the lowest background.

High impedance to external vibration noise manifests in inhibited vibrational coupling of the target (liquid helium) mass to its environment (reservoir walls), due to the distinct superfluid quasiparticle dispersion relation. Finally, application of superfluid helium will exclude any local overheating within a target medium due to its anomalously high thermoconductivity.

Emission spectrum of liquid helium excited by energetic particles spreads over very broad range - from EUV to infrared. It consists of the Hopfield continuum in EUV (from 60 to 100 nm with the maximum at about of 80 nm) and rich spectrum within UV, visible and near infrared spectral (NIR) regions (Stockton et al., 1972; Dennis et al., 1969; Surko et al., 1970). A schematic presentation of an emission spectrum of excited He-II is shown in Figure 1. The spectrum consists of atomic He* lines and excimer He_2* molecule bands. In spite of the apparent simplicity of the electron structure of He_2* molecule, it has a very rich spectrum within the range from ≈300 nm to 2.2 μm in addition to a broad band with the maximum at 80 nm, corresponding to the transitions from the lowest excited singlet and triplet states $A^1\Sigma_u^+$ (18.26 eV) and $a^3\Sigma_u^+$ (17.97 eV) to the unbound ground state $X^1\Sigma_g^+$ (Huber et al., 1979; Hill, 1989). The visible light output of LHe scintillations has been estimated to be at least two orders of magnitude less intense than the EUV output, while the energy conversion efficiency of 160 keV electron beam into EUV photons was estimated as high as 10% (Stockton et al., 1972; Dennis et al., 1969). It is worth to note the radiative relaxation of highly excited ($n \gtrsim 3$) singlet and triplet He atoms, as well as the radiative relaxation of high singlet and triplet states of He_2 molecules shown in Figure 1, were also observed upon excitation of LHe with 160 keV electrons (Dennis et al., 1969; Keto et al., 1974) and 3 MeV protons (Trottier et al., 2000). The life times of the observed atomic transition lie within 1.725 ÷ 94.7 ns for the $3p^1P$ and $3p^3P$ states, respectively (Bukow et al., 1977), while the life times of molecular states are ~10 ns (Neeser et al., 1994).

In condensed helium electrons as well as neutral excited atoms and molecules (of helium and others chemical elements) create bubbles (Fowler and Dexter, 1968; Li et al., 2009), whereas positive ions immediately (at time scale ~100 ps) form snowballs with the effective mass $\approx 45 m_{He}$ (Atkins, 1959; Moroshkin et al., 2008). Hereafter, we will note these snowballs as He^+ or He_2^+.

The time dependence of extreme ultraviolet EUV emission after an ionizing radiation event has been studied in He-II (Benderskii et al., 1999; McKinsey et al., 2003). Four different channels of the emission decay were observed after local ionizations in He-II: 1) a short strong scintillation pulse corresponding to the emission of

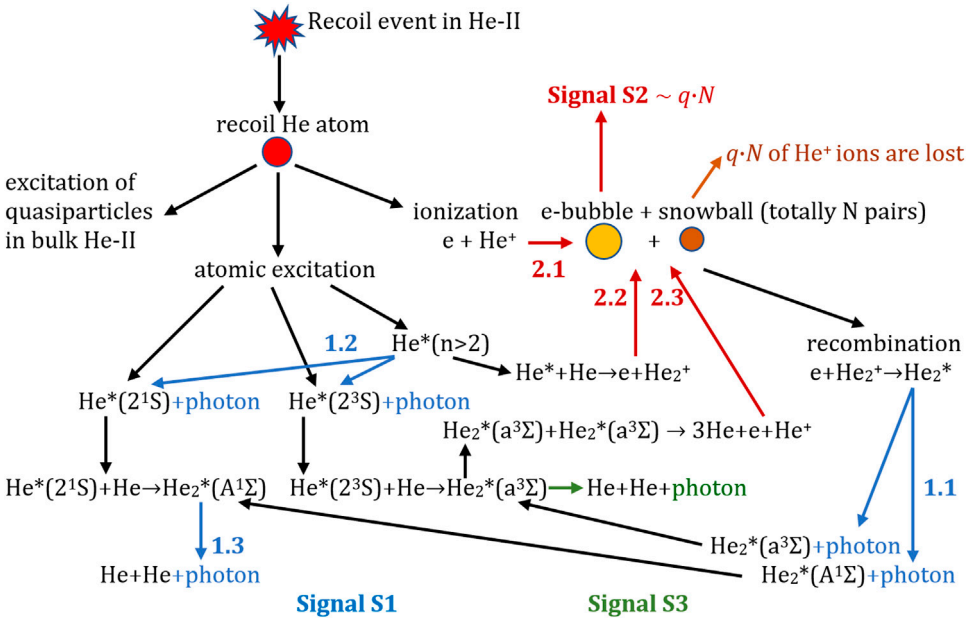

FIGURE 2
The energy pathways in superfluid helium presenting the main channels of the recoil energy dissipation. Blue, dark red, green light arrows, and reaction numbers do correspond to S1, S2, and S3 signals, respectively.

highly excited atoms and molecular excimers emitting within visible and near infrared spectral regions (Figure 1), along with the emission of singlet He_2^* molecule in the lowest bound state $A^1\Sigma_u^+$, with the life time ≈1 ns (Hill, 1989) at wavelength about of 80 nm; 2) a single photon emission with the rate decaying exponentially with a 1.6-μs time constant related to emission from the lowest singlet and triplet states of He_2^* excimer formed due to reactions of remained excited metastable atoms He (2^1 S) and He (2^3 S) with the ground state He ($^1S_0$) atoms; 3) at longer time scale, the emission rate decayed inversely proportional to the time after the initial pulse because of reaction of He_2 ($a^3\Sigma_u^+$) excimers with each other resulting in the Penning ionization; 4) the long-lived decay of He_2 ($a^3\Sigma_u^+$) excimers (McKinsey et al., 1999).

A scheme of the energy pathways in He-II is shown in Figure 2. *N* and *q* correspond to the total number of ion-electron pairs produced due to the recoil event and the fraction of electrons extracted by applied electric field into a gas gap for the electroluminescence detection, the signal S2. Besides of the S1 and S2 signals we show separately the signal S3 due to the long radiative decay of metastable triplets $He_2^*(a^3\Sigma_u^+)$, following to (Guo and McKinsey, 2013). We intentionally do not show any G-values for ionization and excitation processes because their values are variable at nuclear recoil energy below 2 MeV, and become variable at the electron recoil energies below 200 eV, particularly for nuclear recoil (Sato et al., 1976; Toschi et al., 2025). Relative yield of prompt photons, triplet excimers, and quasiparticles (phonons and rotons) determines the sensitivity and discrimination power of a He-II DM detector. Knowledge of the scintillation yields and time dependencies for both nuclear and electronic recoils (Ito and Seidel, 2013; Biekert et al., 2022; Guo et al., 2012) is a crucial point in the design and implementation of future dark matter direct detection experiments with liquid helium. It was estimated (Liao et al., 2023a), that a 1.5 m LHe TPC, the detector size equal to the one used in LUX-ZEPLIN project, with 3 years running can accumulate 1 ton·year exposure and reach the cross-section of ~10^{-45} cm^2 corresponding to the ^{8}B neutrino background (Billard et al., 2014; O'Hare, 2021).

2.2 Porous structures of impurity nanoclusters in He-II

Porous impurity structures are prepared by injection of a gaseous impurity-helium jet in superfluid helium, as shown in Figure 3 (Gordon et al., 1974; Gordon et al., 1993). Chemically active atoms such as H, D, and N are produced in the impurity–helium jets during a passage through a radiofrequency (RF) discharge region (Figure 3A) (Gordon et al., 1993). On the way between the discharge zone and surface of He-II a gaseous impurity-helium jet is cooled by helium vapors which results in formation of impurity nanoclusters. Impurity nanoclusters with size of 3–10 nm are formed upon cooling of a helium jet containing ~ 1% impurity (for instance, atoms of Ne, Ar, Kr, Xe, molecules of hydrogen, deuterium and nitrogen) (Kiselev et al., 2001; Kiryukhin et al., 2007). Nanoclusters with multi-shell structure are formed in cold expanding jets for the case of mixture of impurities with different binding energies (Khmelenko et al., 2012; Danyl et al., 2006). During entering volume of He-II the nanoclusters are quickly captured in He-II volume by quantum vortices and agglomerate into strands (Gordon et al., 2012; Meraki et al., 2017) which tangle and stick together into rather homogeneous porous aerogel-like condensates (Figure 3C). Accumulation of such porous structures which also called impurity-helium condensates (IHCs) does occur in He-II (Figure 3B). The surface of clusters formed by some impurities

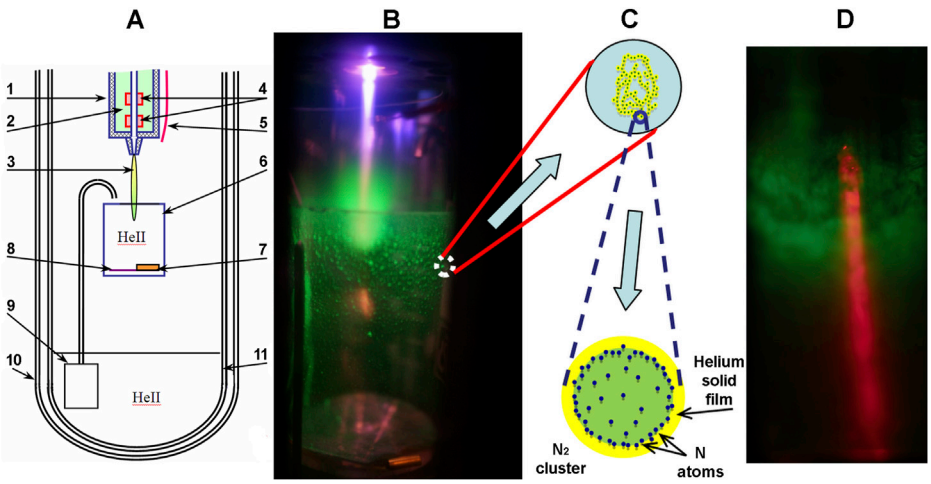

FIGURE 3
(A) scheme of experimental setup for accumulation and investigation of impurity-helium condensates: 1 – atomic source; 2 – liquid nitrogen; 3 – gas jet; 4 – discharge electrodes on a quartz capillary; 5 – optical fiber; 6 – glass beaker filled with He-II; 7 – thermometer; 8 – copper disk; 9 – fountain pump; 10 – nitrogen dewar; 11 - helium dewar; **(B)** photo of the condensation process of the $[N_2]/[He] = 1/100$ gas mixture in He-II. Nitrogen condensate containing N (^{2}D) atoms is seen due to their emission at 523 nm; **(C)** structure of the nitrogen condensate; **(D)** a beam of red laser pointer goes through the beaker filled by porous neon-nitrogen condensate.

(nitrogen, neon and heavier ones) is covered by a layer of adsorbed helium atoms (solid helium). A highly porous structure of these condensates with very broad pore size distributions, from 8 nm up to 860 nm, was revealed by ultrasound attenuation and small-angle x-ray scattering (Kiselev et al., 2001). This porous structure is open for superfluid helium flow. The flow of He-II through the porous structure can be organized by applying gradient of temperature. For velocities of He-II below critical the porous structures will not be disturbed. The impurity densities in condensates immersed in superfluid helium are typically between 0.1%÷5% of the density of liquid helium atoms. These porous structures are typically filled with liquid helium, but their structure mainly remained unchanged even if superfluid helium is removed. However, in order to maintain long term stability of porous structures with trapped chemically active atoms, it is important for the temperature remain lower than the λ-point of ^{4}He.

Impurity condensates were used for studies of the exchange reactions $H_2 + D \rightarrow HD + H$ and $HD + D \rightarrow D_2 + H$ occurring within the hydrogen-deuterium nanoclusters containing atomic deuterium and hydrogen (Gordon et al., 1983; Kiselev et al., 2002). Due to rather large internal surface (~100 m^2/cm^3) and the fact that stabilization of radicals (for example, atomic hydrogen, deuterium or nitrogen) occurs mainly on the surface of impurity nanoclusters separated each from other by adsorbed helium shells (Boltnev et al., 2010), IHCs are of great interest for creation of cryogenic high energy density materials with the local concentrations up to 10^{21} of nitrogen atoms per cm^3 (Bernard et al., 2004; Meraki et al., 2018; Wetzel et al., 2024a). Porous structures consisting of D_2 nanoclusters are perspective materials for production of high-density flux of ultra-cold neutrons via deceleration of very cold neutrons (Mezhov-Deglin et al., 2007; Efimov et al., 2015). Impurity condensates allow to study phase transitions in nanoclusters of noble gases (Krainyukova et al., 2012; Danylchenko et al., 2017) and to observe some exotic complexes and molecules, for example, N^- (Boltnev et al., 2016) and N_4 (McColgan et al., 2017a).

2.2.1 Neon-helium and nitrogen-neon-helium condensates

Neon nanoclusters with typical diameters, R_{cl}, of ≈6 nm (or approximately 5,000 atoms) form rather transparent and homogenous condensates (Figure 3D) with the average atomic neon densities $5{\cdot}10^{20}$ cm^{-3} (Kiryukhin et al., 2007) and pore size distribution from 8 to 320 nm (Kiselev et al., 2001). Within a limited range of deformation, such porous condensates exhibit both solid and liquid characteristics, demonstrating viscoelastic properties (Boltnev et al., 2005; Bari et al., 2024). The neon-helium and nitrogen-neon helium condensates remain stable when submerged in superfluid helium. Warming condensates immersed in liquid helium from 1.5 to 4.2 K results in annealing structural defects and partial recombination of stabilized chemically active atoms in nanoclusters. To initiate structural transformation of neon nanoclusters forming the condensate one has to evaporate all the liquid helium from the condensate and to warm it up to 5 K (Kiryukhin et al., 1997). Aging of the neon-helium condensate in liquid helium at 4.2 K results just in annealing of the cluster structural defects (stacking faults). No changes of the structure of neon-helium condensates was observed during X-ray studies with the energy of photons 17.3 keV. All dissipated energy was efficiently removed by superfluid helium.

From the average density of neon atoms and the mean size of neon nanoclusters, 5,000 atoms, we can estimate the density of neon nanoclusters, n_{cl}, as high as 10^{17} cm^{-3}. The transparent condensates shown in Figure 3 are observable mainly due to green emission from the metastable nitrogen N (^{2}D) atoms. The light scattering in neon-helium condensates with the low content of nitrogen is very weak (Figure 3D), because the index of refraction values for these substances are very small (Table 1).

TABLE 1 Physical properties of liquid helium, solid nitrogen and neon.

Substance	Liquid He	Solid N_2	Solid Ne
Density, g/cm^3	0.1456[a] (@ 2K)	1.032[b]	1.49[c]
Density, atoms/cm^3	$2.19{\cdot}10^{22}$	$2{\cdot}10^{22}$	$4.44{\cdot}10^{22}$
Index of refraction[d], @ 2K	1.029	1.22	1.1
Melting temperature, K	-	77.35[b]	24.7[c]
Ionization energy, eV	24.59[c]	15.58[e]	21.56[c]
Band gap, eV	19.8	15.6	21.5[c]
Mobility of positive ion, cm^2/(V·s)	0.046 (at 4K)[a] 0.35 (at 1.5 K)	0.001[e]	0.02[c]
Mobility of electrons, cm^2/(V·s)	0.02 (at 4K)[a] 0.25 (at 1.5K)	>100[f]	600[g]
Electron affinity, eV	−1[h]	−1.8	−1.3[c]

[a]data from the work (Donnelly and Barenghi, 1998).
[b](Scott, 1976).
[c](Song and Williams, 1996).
[d](Fonda et al., 2016).
[e](Trickl et al., 1989), for gas phase.
[f](Storchak et al., 2001), for α-phase of solid nitrogen.
[g](Loveland et al., 1972).
[h](Sommer, 1964).

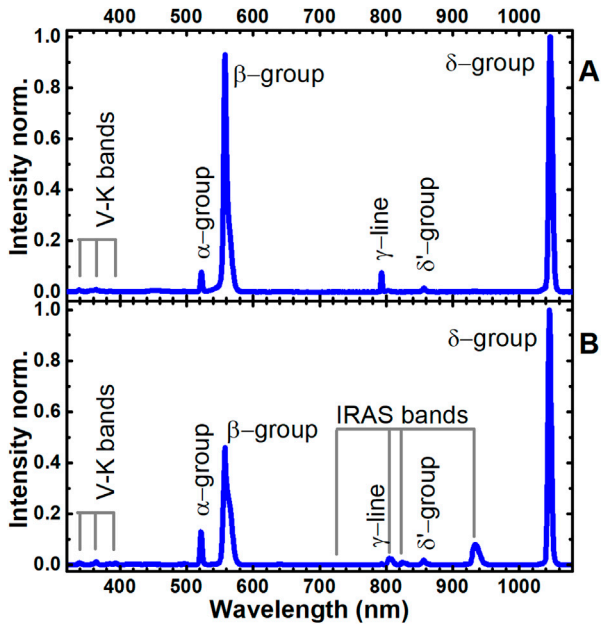

FIGURE 4
Thermostimulated luminescence spectra of neon-nitrogen-helium condensates prepared in He-II from $[N_2]/[Ne]/[He]$ = 1/20/500 **(A)** and $[N_2]/[Ne]/[He]$ = 1/100/10000 **(B)** gas mixtures passed an RF-discharge area (Boltnev et al., 2025).

Rather high average concentration of the nitrogen atoms, n_{av}, can be stabilized in the condensates prepared from gas mixtures with the low nitrogen content. For example, the concentration of N atoms in the condensate prepared from a gas mixture $[N_2]/[Ne]/[He]$ = 1/20/400 passed through a discharge area usually was found as high as $2{\cdot}10^{18}$ cm^{-3} (Bernard et al., 2004; Wetzel et al., 2024b).

Keeping in mind that the majority (≥80%) of N atoms are stabilized on the nanoclusters' surface (Danylchenko et al., 2017), we can find that their quantity on the single cluster surface, n_s, is equal to $(0.8{\cdot}n_{av})/n_{cl} = (0.8 \cdot 2{\cdot}10^{18}\ \text{cm}^{-3})/10^{17}\ \text{cm}^{-3} = 16$. Therefore, about 16 nitrogen atoms reside on the surface of each neon-nitrogen nanocluster.

Warm up of impurity-helium condensates results in evaporation of liquid helium and collapse of their porous structure accompanied by recombination of atoms stabilized on the clusters' surfaces and emission of excited species (Boltnev et al., 1997; Boltnev et al., 2022). Typical thermostimulated luminescence spectra of nitrogen-neon-helium condensates prepared in He-II from $[N_2]/[Ne]/[He]$ = 1/20/500 (Figure 4A) and $[N_2]/[Ne]/[He]$ = 1/100/10000 (Figure 4B) gas mixtures passed an RF-discharge area are shown in Figure 4. One can see emission of molecular nitrogen, so-called Vegard–Kaplan and infrared afterglow system (IRAS) bands corresponding to the transitions ($A^3\Sigma_u^+$,0 → $X^1\Sigma_g^+$,v") and ($B'^3\Sigma_u^-$, v' → $B^3\Sigma_g$, v"), α- and δ-groups of atomic nitrogen related to the transitions N(^{2}D → ^{4}S) and N(^{2}P → ^{2}D), β-group of atomic oxygen due to the transition O(^{1}S → ^{1}D) (Herzfeld and Broida, 1956; Meraki et al., 2016). These transitions are forbidden in the gas phase, but interaction with a matrix of molecular nitrogen greatly enhances their probabilities (Peyron and Broida, 1959). The δ"-group corresponds to the electronic transition N(^{2}P → ^{2}D) accompanied by simultaneous vibrational deexcitation $v = 1 \rightarrow v = 0$ of neighboring nitrogen molecule in the ground state $X^1\Sigma_g^+$ (Herzfeld and Broida, 1956; Oehler et al., 1977). So-called γ-line was assigned to the bound–bound transition ^{1}D → ^{3}P of nitrogen anion N^- formed in matrix as a transient complex during the interaction of delocalized electrons and metastable nitrogen atoms N(^{2}D) (Boltnev et al., 2016). Molecular oxygen is natural admixture in helium gas at the level of a few ppm. Oxygen can be removed by cleaning He gas in a liquid nitrogen trap.

2.2.2 Preparation of impurity condensates

IHCs are usually produced by condensation of impurity-helium gas mixture in bulk He-II (Gordon et al., 1993). The gas flow is about $5{\cdot}10^{19}$ atoms/s. For the gas mixture $[N_2]/[Ne]/[He]$ = 1/500/20000 the flux of neon atoms is equal $\approx 1.25{\cdot}10^{18}$ atoms/s. Then the preparation of 1 cm^3 of neon-nitrogen-helium condensate with average impurity atom density $5{\cdot}10^{20}$ cm^{-3} will take about of 400 s. To accumulate 1,000 cm^3 we need to spend 5 days or to use many atomic sources with the same gas flow value of $5{\cdot}10^{19}$ atoms/s. For instance, 150 atomic sources will be enough to prepare neon-nitrogen-helium condensate with the volume 1 m^3 during 1 month. The high concentrations of nitrogen atoms in the ground state ^{4}S stabilized on the impurity nanoclusters' surface will be prepared by gas mixture passing through an electric discharge area before the accumulation of IHC sample (Figure 3).

2.2.3 Some properties of liquid helium, solid neon and nitrogen

Both liquid helium and neon were discussed as promising low background scintillation media for low energy neutrino detector (McKinsey and Doyle, 2000), as well as for LHe DM detector (Liao et al., 2022) because of their unique properties: large ultraviolet scintillation yields from ionizing radiation, transparency to their own scintillation light, and low levels of radioactive impurities. Some

TABLE 2 The natural abundance and half-life values of the stable and most long-lived isotopes of helium, neon, nitrogen, and argon (for comparison).

Element	Isotope	Natural abundance (Wieser and Coplen, 2010)	Half-life (Kondev et al., 2021)
He	^{3}He	0.000002	stable
	^{4}He	0.999998	stable
	^{6}He		≈0.81 s
N	^{14}N	0.996	stable
	^{15}N	0.004	stable
	^{13}N		598 s
Ne	^{20}Ne	0.9048	stable
	^{21}Ne	0.0027	stable
	^{22}Ne	0.0925	stable
	^{24}Ne		≈203 s
Ar	^{36}Ar	0.00334	stable
	^{38}Ar	0.00063	stable
	^{40}Ar	0.996	stable
	^{37}Ar		35 days
	^{39}Ar	$8{\cdot}10^{-16}$	268 years
	^{42}Ar	$6{\cdot}10^{-21}$	32.9 years

properties of liquid helium, solid nitrogen and neon are listed in Table 1.

Neon and nitrogen, like helium, have no unstable long-lived natural isotopes and therefore no inherent radioactivity, unlike argon, krypton and xenon which have natural radioactivity from the isotopes ^{39}Ar, ^{85}Kr and ^{136}Xe. Neon and nitrogen possess low binding energies to charcoal - the very important opportunity for superior purification by a cold trap. For instance, the impurity content in N_2 gas may by lowered below 10^{-9} by activated carbon absorber at 77 K (Peng et al., 2018). The similar method is used for purification of neon (Harrison et al., 2007). Commercially available neon in the case of contamination with low levels of tritium can be easily cleaned by chemical means (McKinsey and Doyle, 2000). We should also keep in mind that the neon content in bulk He-II will be about of 2% in neon-helium condensate and the nitrogen content ~0.01% in the neon-nitrogen-helium condensate. The stable and most long-lived isotopes of helium, neon, nitrogen, and argon are listed in Table 2 for comparison. As one can see, usage of neon and nitrogen will not affect the extremally low background of main target material–liquid helium-4. For instance, it was estimated that a 3-year run with the 1.5-m size, 330-kg LHe TPC would only have 11 ER and 0.5 NR background events (Liao et al., 2023a).

It was shown that light yields from α- and β-particles induced scintillations in solid neon is higher relative to those in liquid helium at 4.2 K (Michniak et al., 2002). Solid neon absorbs EUV photons mainly within a rather narrow band from 70 to 72 nm (Boursey et al., 1970; Laasch et al., 1990) and scintillates mainly within sharp exitonic lines at around 74 nm and molecular bands within a region from 76 to 80 nm (Fugol' et al., 1972; Schuberth and Creuzburg, 1975). Below $T = 10$ K only a weak maximum at 77 nm can be seen in its spectrum (Fugol' et al., 1972).

Molecular nitrogen absorption bands begin from 60 nm and continue up to 172 nm (Haensel et al., 1971). Emission of molecular nitrogen from nanoclusters is observed mainly within the range from 113 to 420 nm (McColgan et al., 2017b; Boltnev et al., 2025; Savchenko et al., 2019), some discrete lines were also observed at 523 and 1,044 nm due to emission from the metastable states ^{2}D and ^{2}P of a nitrogen atom, as well as at 793 nm–due to emission of nitrogen anion (Boltnev et al., 2016). The cross-sections of molecular nitrogen absorption reach values ~10^{-16} cm^2 within the range 80–100 nm (the Hopfield continuum in the emission of He_2^*), while the cross-section value of atomic nitrogen possesses the maximum ~$1.8{\cdot}10^{-17}$ cm^2 at 650 nm (Ehler and Weissler, 1955) and decreases down to ~10^{-18} cm^2 at wavelengths longer than 750 nm (Gürtler et al., 1977). Therefore, no N_2 molecules should be presented in neon nanoclusters. At high dilution of N_2 in gas mixture the neon nanoclusters containing exclusively N atoms can be formed. EUV photons and energetic electrons excite and dissociate N_2 molecules producing nitrogen atoms in the ground ^{4}S and in the metastable ^{2}D states, with the lifetime in a solid neon matrix equal to ≈360 s (Sayer et al., 1981). We should also note the others features in spectra from excited solid neon doped with nitrogen: three atomic resonant transitions of nitrogen atom from the states 3s ^{4}P and 2p^{4} ^{4}P to the ground one, $^{4}S_{3/2}$, observed at 112.5, and 119.5 nm, as well as 3s ^{2}P → 2p^{3} ^{2}P transition at 173.9 nm (Savchenko et al., 2015).

Some spectroscopic data of principal emitters in liquid helium, solid neon and nitrogen are listed in Table 3. One can see that the lowest quartet states of a nitrogen atom are short-living ones, with life time of order ~ ns, while the lowest doublet states are metastable.

TABLE 3 Transitions, wavelengths and lifetimes of emitters in liquid helium and solid neon.

Substance	Emission	Lifetime, ns	Spectral range, nm
Liquid He	He_2^*, $A^1\Sigma_u^+ \rightarrow X^1\Sigma_g^{+a}$	≈0.55	60÷100
	He_2^*, $a^3\Sigma_u^+ \rightarrow X^1\Sigma_g^{+b}$	$1.3{\cdot}10^{10}$	60÷100
	transitions between excited singlet and triplet states of He* and He_2^{*c}	~10	300÷2,100
Solid Ne	$^1\Sigma_u^+ \rightarrow {}^1\Sigma_g^{+d}$	2.8	74÷75
	$^3\Sigma_u^+ \rightarrow {}^1\Sigma_g^{+d}$	5,200	77
	$3P_2$, a-STE* at a vacancy[d]	3,000	73÷74
	$3P_1$, a-STE* at a vacancy[d]	10	73÷74
	$3P_1$, a-STE* in the bulk[d]	1	73÷74
	N ($^2D \rightarrow {}^4S$)[e]	$3.3{\cdot}10^{11}$	520
	N ($2p^3\ ^2P \rightarrow {}^2D$)[e]	~ 10^7	1,042
	N ($3s\ ^2P \rightarrow 2p^3\ ^2P$)	<10^f	173.9[g]
	N ($3s\ ^4P \rightarrow 2p^3\ ^4S$)	<2.5^f	119.5[g]
	N ($2p^4\ ^4P \rightarrow 2p^3\ ^4S$)	<7.2^f	112.5[g]
	N_2 ($A^3\Sigma_u^+$,0 $\rightarrow X^1\Sigma_g^+$,v")[g]	$3.3{\cdot}10^{9h}$	210–430[g]

[a](Hill, 1989), the gas phase value.
[b](McKinsey et al., 1999).
[c](Bukow et al., 1977; Neeser et al., 1994), the gas phase value.
[d](Fonda et al., 2016).
[e](Kunsch and Dressler, 1978).
[f]gas phase values (Smirnov, 2018).
[g](Savchenko et al., 2015).
[h](Tinti and Robinson, 1968).
*-a-STE, atomic self-trapped exciton.

TABLE 4 The yields of prompt scintillations (S1), charge detection (S2), and He ($a^3\Sigma$) triplet molecules (S3) in different detector target media.

	LHe TPC	3P-TPC Ne	3P-TPC NeN
S1	Prompt scintillation **1.1**[a] - radiative relaxation of highly excited He_2^* dimers **1.2** - radiative relaxation of highly excited He*(n > 2) atoms **1.3** - emission of He_2 ($A^1\Sigma$)	**1.1** + **1.2** +**1.3** **1.4** - Ne-exciton emission due to the energy transfer from He_2^* **1.5** - charge transfer $He^+ + \underline{Ne}^b = He^* + \underline{Ne^+}$ and radiative relaxation of He atom	**1.1** + **1.2** +**1.3** **1.6** - N-exciton emission due to the energy transfer from He_2^* **1.7** - charge transfer $He^+ + \underline{N} = He^* + \underline{N^+}$ and radiative relaxation of He atom
S2	Electroluminescence signal **2.1** – electrons formed within a recoil track **2.2** – electrons – products of the reaction He*(n > 2) + e **2.3** – electrons - products of Penning-ionization $He_2^* + He_2^*$	**2.1** + **2.2** + **2.3**	**2.1** + **2.2** + **2.3** **2.4** - N_2 ($A^3\Sigma_u^+$) emission due to collisions of e-bubbles with nanoclusters **2.5** - N_2 ($A^3\Sigma_u^+$) emission due to quantum vortices
S3	Emission of He_2^* triplet molecules **3.1** - recoil event – He*(n < 3) triplet atoms **3.2** - products of relaxation of highly excited triplet atoms He*(n ≥ 3) **3.3** - relaxed triplet excimers He_2 ($a^3\Sigma$) - products of recombination $He_2^+ + e$	-	-

[a]The bold values (such as 1.1, 1.2, 2.1, etc.) correspond to the reactions shown in Figure 2.
[b]$\underline{Ne}$ and $\underline{N}$, $\underline{Ne^+}$ and $\underline{N^+}$ are the neon and nitrogen atoms and ions residing on the nanocluster surface, correspondingly.

3 Basic principles of 3P-TPC

We propose two versions of 3P-TPC: the fiducial volume of the first one, 3P-TPC Ne, will be filled with He-II and pure neon nanoclusters, while the fiducial volume of the second, 3P-TPC NeN, will be filled with He-II and neon-nitrogen nanoclusters. Signal partitioning in LHe TPC (following to the Figure 2), 3P-TPC Ne, and 3P-TPC NeN, is listed in Table 4. The reaction (pathway) numbers correspond to the ones shown in Figure 2 for the dissipation of recoil energy in pure He-II. As one can see the main difference of the proposed target media is fast conversion (within ~ μs instead of ~10 s) of the energy stored in metastable triplet molecules into photons emitted by Ne-excitons (reaction 1.4) or nitrogen atoms in nanoclusters (1.6). There are two dominant processes of relaxation from the lowest exciton state in pure neon crystal: the radiative decay of free exciton or exciton self-localization followed by luminescence. In the case of the presence of an impurity center (a nitrogen atom) with lower value of the band gap, it can be regarded as a deep trap and exciton localizes at the impurity (Fonda et al., 2016). Thus, the energy will be transferred to a nitrogen atom which decays through a cascade of the transitions some of which can be optically detected (Table 3).

Moreover, both versions of 3P-TPC will use the He^+ ions extracted from the recoil track. Helium atom has the highest ionization potential among all chemical elements. Some part of positive ions He^+ formed during the recoil event will meet the nanoclusters and ionize them through a charge transfer from He^+, which is a state-to-state process (Bonhommeau et al., 2006; Ruchti

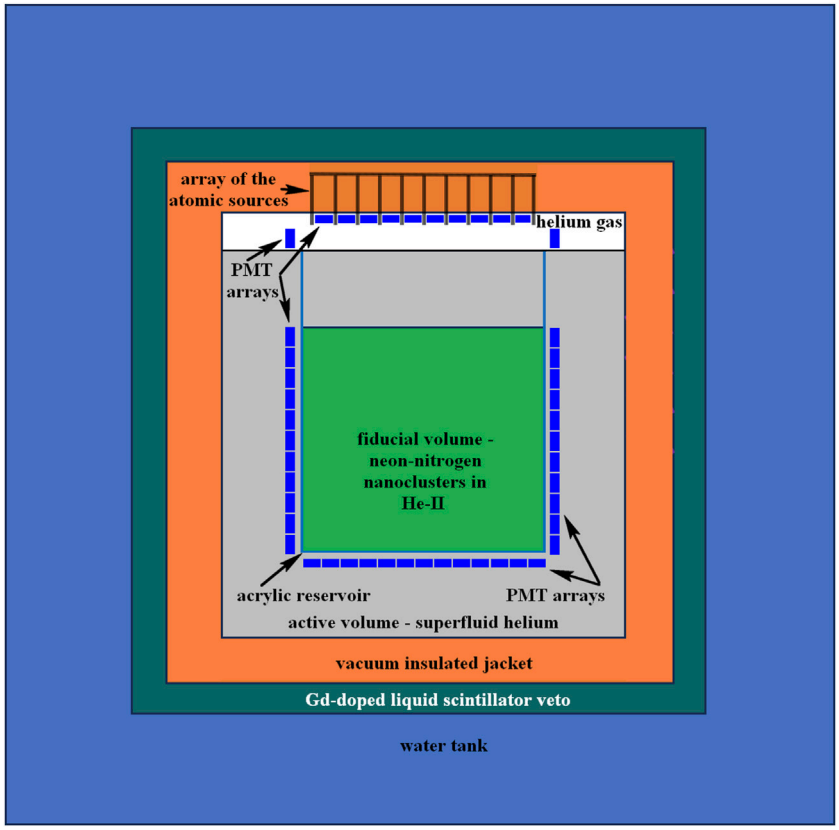

FIGURE 5
The schematic drawing of the 3P-TPC (not to scale). From outside to inside: The blue area corresponds to the water tank surrounding the whole detector system, with a thickness of a few meters; the dark green is related to the Gd-doped liquid scintillator veto, with the thickness of ~ half-meter; the orange area corresponds to thermal insulation gap; the grey area is related to the self-shielding layer of the active volume of the TPC, filled with superfluid helium, where the green region represents the fiducial volume with neon-nitrogen nanoclusters immersed in He-II and confined by acrylic parallelepiped open from the top, with the base 1 × 1 m, and height 1 m. The five arrays of PMTs (shown by dark blue) for detection a prompt scintillation signal will be located directly in superfluid helium around to the acrylic reservoir. Two arrays of PMTs will be located above bulk He-II in the active volume of TPC to detect an electroluminescence signal. The top array PMTs alternate mosaically with the atomic sources. PMTs for detection of background signals inside of the water tank and scintillation inside of the veto detector are not shown here.

et al., 1998). As a result, neutralized He* atoms (1.5 and 1.7) appear instead of non-emitting He^+ ions. Ne or N atom ionized through a charge transfer, may later recombine with a drifting electron and form an exciton with fast emission of photon.

We emphasize that a major part of the recoil events in liquid helium relates to generation of quasiparticles (phonons and rotons) and quantum vortices, particularly within the recoil energy range of interest 100 eV_{NR} - 10 keV_{NR} (Toschi et al., 2025). It was shown, that the luminescence of nanoclusters doped with N atoms and immersed in He-II may be induced by quantum vortices (Meraki et al., 2017; McColgan et al., 2019). The nitrogen atoms stabilized on the neighbor clusters' surface do recombine if the clusters come in contact due to any rearrangement of such nanoclusters caused by interaction with drifting electron bubble or quantum vortex. Therefore, the porous condensates consisting of neon nanoclusters doped with N atoms (see Section 2.2.2) will be sensitive to local appearance of quantum vortices within the recoil track and may be sensitive to the motion of electron bubbles in He-II (2.5 and 2.4 in Table 4).

3.1 Construction of 3P-TPC

A detailed project of the 3P-TPC has to be elaborated on the basis of present knowledge about functioning two-phase liquid noble gas TPCs, and, particularly, new information gathered during step by step development the ALETHEIA project (Liao et al., 2022; Liao et al., 2023a; Gu et al., 2024).

Comparing to the radioactive background from the construction materials of the detector, background external to the detector (excluding neutrino background) can be reduced simpler by passive shielding and active veto detector. Anti-coincidence veto detectors usually surround the detector to determine the remaining background. DM detectors are placed in deep underground laboratories to shield against cosmic rays. For example, the muon flux can be reduced down to ~10^{-6} or even ~10^{-9} part, depending on the depth. Several layers of shielding are needed to minimize ambient radioactivity from the rock and the concrete in underground laboratories. To attenuate γ-rays steel and lead are often employed. Water and low-Z materials are employed to attenuate neutrons.

Figure 5 presents a schematic drawing of a 3P-TPC. The TPC center is green area, representing the fiducial volume (filled with superfluid helium-4 and neon-nitrogen nanoclusters), where extremely low or zero background is expected. It corresponds to the cube with the side length of 1 m inside an acrylic parallelepiped open from the top. The active volume of the detector is presented by white and grey–gaseous and superfluid helium, respectively. The gap between the parallelepiped wall and the vacuum insulated jacket (orange) as well as the He-II layer between gas phase and the fiducial volume are related to the self-shielding layer (grey). A Gd-doped scintillator detector (dark green) acts as a veto. A water tank (blue) with a few meters thickness is designed to thermalize neutrons and γ-rays outside of the detector system. A typical WIMPs signal would only have one hit registered due to a very weak coupling between WIMPs and helium nuclei. The neutrons and γ-rays from inside of the TPC can be discriminated by S1/S2 or PSD (Pulse Shape Discrimination) analysis from nuclear recoils induced by a WIMPs.

As was estimated before, about 150 atomic sources will be needed for accumulation of porous condensate over 1 m^3 of He-II. Exit orifices of the source should be at the height 25–30 mm above the He-II level in the camera. A construction of an atomic source is rather simple: a stainless steel capillary surrounded by a vacuum jacket with a heater at the bottom end with output orifice and dielectric thermal screen (Kiselev et al., 2001). The total gas flow (for a gas mixture [Ne]/[He] = 1/40 or $[N_2]$/[Ne]/[He] = 1/500/20000) will be equal to $150{\cdot}5{\cdot}10^{19} = 7.5{\cdot}10^{22}$ atoms/s. For dissociation of nitrogen molecules will be used electric discharge. Electrodes for initiation of corona discharge will be attached to the dielectric screen. A top electrode for electroluminescence stimulation has to be under zero electric potential, as at the atomic sources, to avoid development of gas discharge. It was shown, that intense electroluminescence (S2 signal) can be generated under the voltage of 500 V/cm in dual-phase TPC filled with LHe (Sethumadhavan, 2007). Here we will focus on new, specific, requirements dictated by the proposed conception. Some of them need to be tested and developed. We suggest that the active volume of the TPC will be filled with the He-II, while the fiducial volume will be filled by superfluid helium and neon-nitrogen condensate.

Atomic sources manifold will be located above the He-II bulk for preparation of neon-nitrogen condensate. The saturated vapor pressure of helium gas at 1.5 K is about of 470 Pa (Donnelly and Barenghi, 1998). At such pressures the corona discharge can be easily initiated by applying rather low ~100 V negative potential between a sharp tungsten tip with the radius of curvature ≤1 μm (Golov and Ishimoto, 1998) and an open grounded metallic surface (Boltnev et al., 2022).

A construction of 3P-TPC must provide the efficient collection of scintillations produced both by excitation and ionization. The arrays of the photomultiplier tubes (PMTs) will collect photons emitted by excited atoms He* and excimer molecules He_2*, emission of excitons, atomic and molecular nitrogen from nanoclusters (Table 3) within a visible spectrum range along with photons reemitted by tetraphenyl butadiene (TPB). Thin (with the thickness ~ μm) films of TPB are traditionally used for conversion ultraviolet emission into visible light within the range from 390 to 520 nm (with the maximum at 425 nm). It was found that TPB at temperatures of ~1 K possesses even higher photoluminescence efficiency than at room temperature (Francini et al., 2013). The intrinsic quantum efficiency of TPB thin films, defined as the probability that a photon absorbed by a TPB film is reemitted, is equal to 30÷40% within the spectral range from 60 to 100 nm and reach 70% within the range 100–200 nm (Benson et al., 2018). The inner surface of the UV transmitting acrylic parallelepiped will be covered by a TPB layer with the thickness of 3 μm. The efficiency of light collection for the PMTs arrays located accordingly to Figure 5 is about 35%.

PMTs Hamamatsu R8520-06 may be used for detection of photons. This model of PMT possesses the maximum of quantum efficiency about 30% matching to the TPB luminescence maximum and can be used in He-II environment (Biekert et al., 2022). The spectral range of PMT R8520-06 covers wavelengths from 160 up to 650 nm and allows to detect emission of excited helium species within the visual spectral range besides of the TPB emission. Five arrays of PMTs around the fiducial volume (Figure 5) confined by an acrylic parallelepiped (without a top side) will provide the light collection efficiency ≈35%. Two top arrays of PMTs will collect electroluminescence signal with the similar efficiency. Totally, approximately 9,000 PMTs will be needed for the light detection system configuration shown in Figure 5.

Due to the high thermal conductivity of He-II, its temperature in active and shielding areas will be easily kept the same and very stable. The temperature of He-II will be kept constant by pumping rate of helium vapor.

3.2 Problematic topics of the suggested concepts

Up to date there are no experimental or theoretical results concerning an electron drift through any porous structures (aerogels widely used to study properties of condensed helium-4 and helium-3, or impurity-helium condensates). Nevertheless, there are two factors favorable for electron motion through neon-nitrogen-helium condensate: the larger negative values of the electron affinity of solid nitrogen and neon comparing to that of liquid helium (Table 1) – an electron should remain in He-II during its drift and do not "stick" to the solid impurity structure, and the high porosity of the condensate–impurities occupy only ≈1% of the total volume. A diameter of electron bubble in He-II, ≈3.8 nm, is rather small comparing to pore size in neon-nitrogen-helium condensates with the broad pore size distribution from 8 to 320 nm (Kiselev et al., 2001) allow us to conclude about their permeability for drifting electrons. We should mention that drift of electrons in bulk He-II under strong electric field gradient (~kV/cm) within the temperature range $1\text{K} < T < 1.8$ K may result in the nonlinear dependency of the drift velocity on the applied electric field. Moreover, reaching the critical velocity at electric field >5 kV/cm causes generation of vortex rings and sharp decrease of the electron velocity (Reif and Meyer, 1960).

There is still open question with the optical detectability of highly excited N atom in a neon nanocluster: there are many pathways, but which fraction of them follow to radiative decay is not clear. Nevertheless, we know that three transition are observable within 110–190 nm spectral range, as well as the transition ^2P-^2D at λ = 1,044 nm.

As the first stage of the project (2025–2026) we plan to carry out some preliminary experiments in a smaller scale of an experimental cell (volume ~30 cm^3):

1. The investigations of electron mobility through He-II in the pores of neon-nitrogen-helium condensates. The dependences of the electrons mobility in the condensates on applied electric field and on the porosity of the condensates should be investigated.
2. The study of the detection efficiency of drifting electron via detection of emission of excited nitrogen molecules initiated either by collisions of the electron with neon-nitrogen nanoclusters or by interaction of quantum vortices with the nanocluster porous structure.

We are looking for any collaboration to carry out also such experiments as:

3. Investigation of prompt light pulse transformation within the neon-nitrogen-helium condensates: we expect some temporal extension of the pulse peak due to emission of neon/nitrogen atoms excited by triplet He_2* molecules and excited He* atoms formed in a process of neutralization of He^+ ions.
4. Analysis of S2/S1 ratio discrimination of nuclear/electron events for low recoil energies (below 20 keV) with the G(E) values for atomic ionization and excitation, quasiparticle excitation dependences for electrons and helium nuclei in bulk He-II.
5. Direct experimental comparison of the temporal dependences of the EUV prompt scintillation and the luminescence within visible and NIR spectral ranges. The experiment should be carried out in normal LHe (at $T > 2.2$ K), in pure He-II (at $T < 2$ K), in He-II with neon-helium condensate, and in He-II with neon-nitrogen-helium condensate.

4 Discussion

A light DM particle scattering event in LHe would result a recoil helium atom. The energy of the recoil helium atom is expected to be low, less than 100 keV. Dissipation of the recoil atom energy through collisions with He atoms in the ground state may lead to their excitation and ionization. The helium atom in (1s2p) state with energy of 21.2 eV is the most probable product of such low energy collisions (Kempter et al., 1975). The fraction of singly charged ions, He^+, was estimated about a few percent and ~0.01% at the recoil energies 10 and 1 keV (Guo and McKinsey, 2013), respectively, while the neutral He* atom is dominant at recoil energy below 100 keV (Talman and Frolov, 2006). About 60 prompt scintillation photons (S1) and 22 electrons (S2) were estimated for a recoil He atom with energy 5 keV in an electric field of 10 kV/cm. Each energetic particle moving through LHe produces ionization and excitation of helium atoms along its trajectory. The recoil track length in LHe at 1.75 K is about 40 μm for 1 MeV recoil α-particle (a helium nuclei) and about 3 mm for 200 keV recoil electrons (Biekert et al., 2022). The average energy needed for production of an electron-ion pair by an energetic electron and α-particle is about 42.5 eV (Jesse and Sadauskis, 1955). Thus, ionization events will be separated by 640 nm away from each other along the electron recoil track and 1.7 nm along the α-particle recoil track. The fraction of the electrons that can be extracted under an applied electric field depends strongly on the initial electron-ion separation and the ionization density along the projectile track. The mean electron-ion separation has been determined to be about 60 nm for ionization events caused by both beta particle (Guo et al., 2012) and alpha particle (Ito et al., 2012). Due to the shorter distance between ionization events along the α-particle recoil track the ionization density in this case is much higher. Nevertheless, due to the Lindhart effect, a main part of the recoil energy of helium nuclei dissipates in elastic collisions at low energies: for 10 keV and lower the ionization events separated by about 20 nm and longer distances, respectively. Thus, the mean electron-ion separation along the track of a low energy recoil He nuclei becomes similar to that for beta particles and comparable with pore sizes within the neon-helium condensate.

The situation is drastically changed if porous structure composed by neon nanoclusters is immersed within bulk He-II. For easier classification of the energy dissipation channels, the yields of prompt scintillations (S1), charge detection (S2), and He_2 ($a^3\Sigma$) triplet molecules (S3) in different detector target media discussed here are listed in Table 4. LHe TPC, 3P-TPC Ne and 3P-TPC NeN correspond to the detectors with the target media made of liquid helium, He-II with neon nanoclusters, and He-II with neon-nitrogen nanoclusters, containing stabilized N atoms, respectively.

The main feature which determines the diffusion in any kind of porous disordered medium is not its structure, but rather the configuration of the interconnected pores accessible for a moving particle. The accessibility of pores depends on the particle effective size, R_{eff}, and can be determined by chord length distribution analysis (Torquato and Lu, 1993). For an electron bubble, with R_b = 1.9 nm (Ghosh and Maris, 2005) moving through porous medium consisting of monodisperse neon nanoclusters, the bubble effective size $R_{eff} = (R_b + R_{cl})/2 \approx 2.5$ nm.

Chords are direct lines restricted by intersections with the two-phase interfaces. The microstructure of two-phase random porous media is characterized by the chord-length distribution function, which gives us information of the length scales of the obstacle structures. The first momentum of the chord-length distribution function, l_m, is related to mean chord length (Torquato and Lu, 1993). For 3-dimensional space we get the value $l_m \approx 500$ nm from the formula

$$l_m = (1-\eta)/(\pi \cdot R_{eff}^2 \cdot n_{cl})$$

where $\eta \approx 0.01$ is the volume fraction occupied in He-II by neon nanoclusters. Therefore, the average distance passed by an electron bubble between collisions with the nanoclusters is about of 500 nm. During the drift an electron gains the energy from the electric field. For E = 1 kV/cm, the gain of electron energy is equal to $e{\cdot}E{\cdot}l_m$ = 50 meV. Transfer of this energy during collisions to neon-nitrogen nanoclusters may result in their rearrangements and recombination of nitrogen atoms in the ground state $N(^4S)$ – channel 2.4 (Table 4). The product of the recombination is exclusively the lowest excited state of molecular nitrogen–$A^3\Sigma_u^+$ with the radiative lifetime 3.3 s (Table 3).

It is worth to mention also, that the energy of formation of a vortex ring with the radius equal to the electron bubble radius is ≈3 meV (Rayfield and Reif, 1964; Sullivan et al., 2008). The

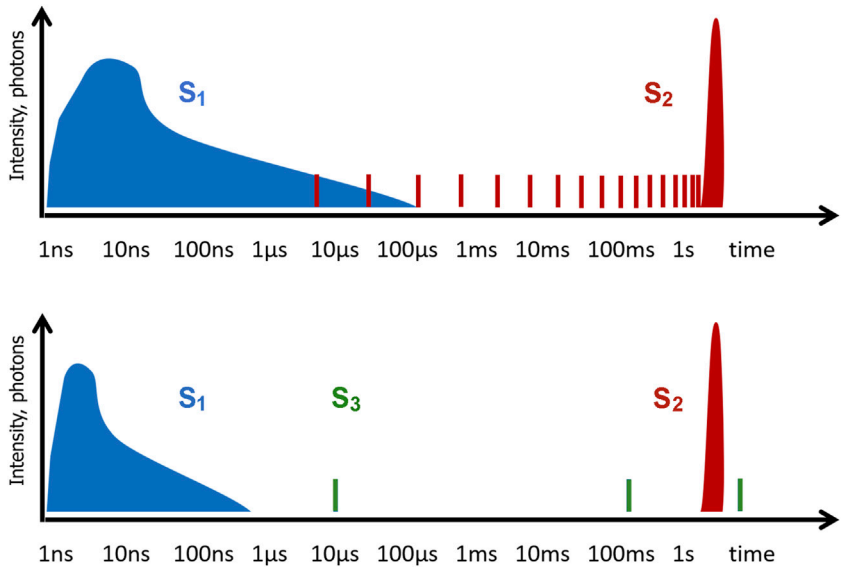

FIGURE 6
Expected recoil event signals: in proposed 3P-TPC NeN (top); and in 2-phase LHe TPC (bottom). Signals S1, S2, and S3 are marked by blue, red, and green colors, respectively.

appearance of quantum vortices in neon-nitrogen condensates containing stabilized N atoms results in their recombination (Meraki et al., 2017; McColgan et al., 2019) – channel 2.5. Therefore, the $N_2(A^3\Sigma_u^+)$ emission can be initiated by two different mechanisms due to electron drift in porous condensates with high density of N atoms stabilized on the neon nanoclusters' surface.

A key aspect of the proposed detector is the optical detection of enhanced S1 and S2 signals (Figure 6). Enhancement of S1 signal is provided by localization of the recoils event within pores of the impurity-helium condensate. It applies the limit on the drift time of excimer molecules He_2^*. From the equation $< x^2> = 2{\cdot}D{\cdot}t$

which expresses the mean squared displacement, $<x^2>$, in terms of the time elapsed, t, and the diffusion coefficient, D, we can find that the displacement of a Brownian particle is proportional to a square root of the elapsed time. If we estimate the displacement value equal to 500 nm: then He_2^* metastable molecules moving as Brownian particles with the diffusion coefficient $3{\cdot}10^{-4}$ cm^2/s (Calvani et al., 1974) will overcome this distance in

$$t = 25 \cdot 10^{-10} / \left(2 \cdot 3 \cdot 10^{-4}\right) \approx 4 \cdot 10^{-6} = 4\,\mu s$$

Therefore, the energy carried out by excimer molecules He_2^* will be efficiently transferred to neon-nitrogen-helium condensate within a few of μs to induce emission of photons within ~10 μs instead of ~13 s (Table 3), channels 1.4 and 1.6 (Table 4). Such an energy conversion mechanism will also diminish the number of He_2^* molecules which participate in bimolecular reaction resulting in the Penning ionization. We should mention that product of the Penning ionization–a thermalized helium ion He^+ quickly forms a snowball in LHe and doesn't emit itself without recombination with an electron. In the neon-nitrogen-helium condensate a positive ion He^+ generated during the recoil event will be quickly neutralized by the impurity nanocluster due to a charge transfer either to N or Ne atom (channels 1.5a and 1.7a, respectively, in Table 4), as it occurs with the guest molecules in nanodroplets of He-II (Moon et al., 2023). It is well known, that an addition of nitrogen and oxygen colloidal particles drastically enhances the luminescence intensity of liquid helium within the range 200–600 nm (Jortner et al., 1964). The emission of impurity atoms and molecules may be explained by two processes: formation of excited molecules of nitrogen due to a direct absorption of EUV photons by the molecules and the energy transfer from metastable excited helium species (triplet molecules) to the impurity clusters (Mehrotra et al., 1979; Popov et al., 2005). We suggest that EUV photon absorbed by a neon cluster may be either reemitted by a neon exciton (Fonda et al., 2016) or exciton energy will be transferred to nitrogen atom. The exciton diffusion length in solid neon, ~10 nm (Laasch et al., 1990), is substantially larger of the neon cluster' size. The exciton energy, ≈16.7 eV, is high enough to excite or ionize a nitrogen atom. The possibility of this mechanism is proved by the luminescence spectra of liquid helium doped with nitrogen and oxygen colloidal particles (Jortner et al., 1964) - the intense luminescence of the Vegard-Kaplan bands of molecular nitrogen and the α-group of the nitrogen atoms was observed.

Hence, 3P-TPC allows to enhance the S1 signal due to 2 different channels (see Table 4): the additional emission from He^* atoms produced by neutralization of He^+ ions with neon or neon-nitrogen clusters (usually in pure LHe the He^+ ions drawn away from the ionization track by electric field don't give any input to the signals S1 and S2); the exciton luminescence from the neon or neon-nitrogen nanoclusters initiated by energy transfer to the clusters from He_2^* molecules.

There are two ways to increase the S2 signal which are related to condensates made of mixed neon-nitrogen nanoclusters. They are based on conversion of chemical energy stored in nitrogen atoms into emission of N_2 molecules produced by the atomic recombination. The nitrogen atoms recombination can be stimulated either by quantum vortices or by drifting electron

bibbles (see Table 4). The formation of quantum vortices is caused by excitation of He-II within the ionization track, while the drifting electron bubbles colliding the nanoclusters may rearrange them and initiate the recombination of N atoms residing of the surface.

Expected recoil event signals S1, S2, and S3 for the proposed 3P-TPC NeN and for 2-phase LHe TPC are shown in Figure 6, top and bottom parts, respectively. The signal S3 will be converted into S1 in 3P-TPC NeN, as well as in 3P-TPC Ne (Table 4).

Using the calculations carried out for the 330-kg LHe detector (Liao et al., 2023a), we can estimate background of the proposed 3P-TPC with the fiducial volume of 1 m^3 and mass about of 160 kg as high as 2 ER and 0.1 NR background events per 1-year run.

We suggest that a three-phase TPC will provide the possibility to tune the balance between the S1 and S2 values by changing the electric filed value applied to the drift region. There is a direct connection between the charge collection efficiency and the prompt scintillation signal: the higher value of charge extracted–the weaker scintillation and *vice versa*.

It is worth to mention that some part of photons (within visual and NIR spectral range) is lost for detection since PMTs used possess "reg limit" at 600–650 nm. We suggest that in the case detection of photons from excited He-II this part of spectrum (600–2,200 nm) has to accounted also for obtaining stronger S1 signal.

The 3P-TPC NeN provides stronger signal S2, but the presence of nitrogen atoms in the target media can affect signal S1 due to rather strong absorption of nitrogen atoms within the spectral range below 75 nm (cross-section $\approx 10^{-17}$ cm^2). There is no information concerning the reemission efficiency of N atoms and we do not know which part of absorbed photons will be reemitted through the resonance transitions (Table 3). This problem as well as the drift of electron bubbles through porous structures in He-II have to be studied as soon as possible.

5 Conclusion

A new concept of three-phase projection chamber filled with a collection of neon-nitrogen nanoclusters immersed in superfluid helium-4 is proposed for detection light dark matter particles with low masses (0.1–10 Gev/c^2). The proposed concept of three-phase TPC will allow to enhance both the signals S1 and S2 needed for distinguishing between electron and nuclear recoils. The enhancement of S1 signal will be provided by fast (within ~ μs) energy transfer from He_2^* metastable triplet molecules to neon (neon-nitrogen) nanoclusters and the exciton emission. The positive ions He^+ drown away of the recoil track by electric filed will be neutralized via charge transfer to nanoclusters. The excited He* atoms radiatively relax to the states 2^1S and 2^3S, and become the precursors for singlet and triplet He_2^* molecules. Nitrogen atoms stabilized in neon-nitrogen nanoclusters can give additional gain to S2 signal via emission of $N_2(A^3\Sigma_u^+)$ molecules produced due to nitrogen atoms recombination activated either by electron bubbles drifting through the detector target medium or thermal excitation and quantum vortices generation within the recoil track. A combination of He-II with porous structure formed by neon-nitrogen nanoclusters will enhance the S1 and S2 signals in comparison with LHe detector and doesn't affect its ultralow background.

Data availability statement

The raw data supporting the conclusions of this article will be made available by the authors, without undue reservation.

Author contributions

RB: Conceptualization, Visualization, Writing – original draft, Writing – review and editing. VK: Conceptualization, Writing – review and editing.

Funding

The authors declare that financial support was received for the research and/or publication of this article. VVK wishes to acknowledge the support by the National Science Foundation (NSF) through Grant #DMR 2104756.

Conflict of interest

The authors declare that the research was conducted in the absence of any commercial or financial relationships that could be construed as a potential conflict of interest.

Generative AI statement

The authors declare that no Generative AI was used in the creation of this manuscript.

Publisher's note

References

Aalbers, J., Akerib, D., Akerlof, C., Al Musalhi, A., Alder, F., Alqahtani, A., et al. (2023a). First dark matter search results from the LUX-ZEPLIN (LZ) experiment. *Phys. Rev. Lett.* 131, 041002. doi:10.1103/PhysRevLett.131.041002

Aalbers, J., Akerib, D., Musalhi, A. A., Alder, F., Alsum, S., Amarasinghe, C., et al. (2023b). Background determination for the LUX-ZEPLIN dark matter experiment. *Phys. Rev. D.* 108, 012010. doi:10.1103/PhysRevD.108.012010

Abrikosova, I. I., and Shal'nikov, A. I. (1971). The purity of liquid helium. *Cryogenics* 11, 137–138. doi:10.1016/0011-2275(71)90295-5

Acharya, P., Fritts, M., Mei, D.-M., Wang, G.-J., Mahapatra, R., and Platt, M. (2024). Exploring charge transport dynamics in a cryogenic P-type germanium detector. *J. Phys. G Nucl. Part. Phys.* 51, 095001. doi:10.1088/1361-6471/ad60e6

Adams, J. S., Bandler, S. R., Brouër, S. M., Lanou, R. E., Maris, H. J., More, T., et al. (1995). Simultaneous calorimetric detection of rotons and photons generated by particles in superfluid helium. *Phys. Lett. B* 341, 431–434. doi:10.1016/0370-2693(95)80025-s

Aprile, E., Abe, K., Agostini, F., Ahmed Maouloud, S., Althueser, L., Andrieu, B., et al. (2023). First dark matter search with nuclear recoils from the XENONnT experiment. *Phys. Rev. Lett.* 131, 041003. doi:10.1103/PhysRevLett.131.041003

Atkins, K. R. (1959). Ions in liquid helium. *Phys. Rev.* 116, 1339–1343. doi:10.1103/PhysRev.116.1339

ATLAS and CMS collaborations (2022). Searches for dark matter with the ATLAS and CMS experiments using LHC run 2 (2015–2018) data. *PoS PANIC2021*. doi:10.22323/1.380.0137

ATLAS and CMS collaborations (2025). Searches for top-associated dark matter production at the LHC. arXiv.2501.06072. doi:10.48550/arXiv.2501.06072

Baer, H., Choi, K.-Y., Kim, J. E., and Roszkowski, L. (2015). Dark matter production in the early Universe: beyond the thermal WIMP paradigm. *Phys. Rep.* 555, 1–60. doi:10.1016/j.physrep.2014.10.002

Baker, C. G., Bowen, W. P., Cox, P., Dolan, M. J., Goryachev, M., and Harris, G. (2024). Optomechanical dark matter instrument for direct detection. *Phys. Rev. D.* 110, 043005. doi:10.1103/PhysRevD.110.043005

Bari, G. A., Jeong, J.-H., and Barai, H. R. (2024). Conductive gels for energy storage, conversion, and generation: materials design strategies, properties, and applications. *Materials* 17, 2268. doi:10.3390/ma17102268

Benderskii, A. V., Zadoyan, R., Schwentner, N., and Apkarian, V. A. (1999). Photodynamics in superfluid helium: femtosecond laser-induced ionization, charge recombination, and preparation of molecular Rydberg states. *J. Chem. Phys.* 110, 1542–1557. doi:10.1063/1.477796

Benson, C., Orebi Gann, G. D., and Gehman, V. (2018). Measurements of the intrinsic quantum efficiency and absorption length of tetraphenyl butadiene thin films in the vacuum ultraviolet regime. *Eur. Phys. J. C* 78, 329. doi:10.1140/epjc/s10052-018-5807-z

Bernard, E. P., Boltnev, R. E., Khmelenko, V. V., and Lee, D. M. (2004). Stabilization of high concentrations of nitrogen atoms in impurity-helium solids. *J. Low Temp. Phys.* 134, 199–204. doi:10.1023/B:JOLT.0000012556.69060.eb

Bertone, G., Hooper, D., and Silk, J. (2005). Particle dark matter: evidence, candidates and constraints. *Phys. Rep.* 405, 279–390. doi:10.1016/j.physrep.2004.08.031

Bhattarai, S., Mei, D., Raut, M. S., Panth, R., Kooi, K., Mei, H., et al. (2023). Investigating binding energies and trapping cross-sections in an n-type Ge detector at low temperatures. *Front. Detect Sci. Technol.* 1, 1275385. doi:10.3389/fdest.2023.1275385

Biekert, A., Chang, C., Fink, C., Garcia-Sciveres, M., Glazer, E., Guo, W., et al. (2022). Scintillation yield from electronic and nuclear recoils in superfluid He-4. *Phys. Rev. D.* 105, 092005. doi:10.1103/physrevd.105.092005

Billard, J., Figueroa-Feliciano, E., and Strigari, L. (2014). Implication of neutrino backgrounds on the reach of next generation dark matter direct detection experiments. *Phys. Rev. D.* 89, 023524. doi:10.1103/physrevd.89.023524

Boltnev, R. E., Bernard, E. P., Jarvinen, J., Krushinskaya, I. N., Khmelenko, V. V., and Lee, D. M. (2010). Stabilization of H and D atoms in aggregates of Kr nanoclusters immersed in superfluid helium. *J. Low. Temp. Phys.* 158, 468–477. doi:10.1007/S10909-009-9961-4

Boltnev, R. E., Bykhalo, I. B., and Krushinskaya, I. N. (2022). Impurity systems in condensed helium-4. *J. Low. Temp. Phys.* 208, 50–66. doi:10.1007/s10909-021-02617-4

Boltnev, R. E., Bykhalo, I. B., Krushinskaya, I. N., and Pelmenev, A. A. (2025). Emission of N_2 $B'^3\Sigma_u^- \rightarrow B^3\Sigma_g$ from solid neon doped by nitrogen. *High. Energy Chem.* 59, 154–159. doi:10.1134/S0018143924701662

Boltnev, R. E., Bykhalo, I. B., Krushinskaya, I. N., Pelmenev, A. A., Mao, S., Meraki, A., et al. (2016). Spectroscopic observation of nitrogen anions N^- in solid matrices. *Phys. Chem. Chem. Phys.* 18, 16013–16020. doi:10.1039/c6cp01080f

Boltnev, R. E., Gordon, E. B., Krushinskaya, I. N., Martynenko, M. V., Pelmenev, A. A., Popov, E. A., et al. (1997). Analysis of decomposition of impurity-helium solid phase. *Low. Temp. Phys.* 23, 567–577. doi:10.1063/1.593424

Boltnev, R. E., Karabulin, A. V., Krushinskaya, I. N., Pelmenev, A. A., and Matyushenko, V. I. (2023). Ionization of helium atoms by triply charged metal atoms during laser ablation of metals in superfluid helium. *High. Energy Chem.* 57, 168–173. doi:10.1134/S0018143923020066

Boltnev, R. E., Krushinskaya, I. N., Pelmenev, A. A., Popov, E. A., Stolyarov, D. Yu, and Khmelenko, V. V. (2005). Study of the stabilization and recombination of nitrogen atoms in impurity-helium condensates. *Low. Temp. Phys.* 31, 547–555. doi:10.1063/1.2001631

Bonhommeau, D., Halberstadt, N., and Viel, A. (2006). Fragmentation dynamics of ionized neon clusters (Ne_n, n=3–14) embedded in helium nanodroplets. *J. Chem. Phys.* 124, 024328. doi:10.1063/1.2158993

Boursey, E., Roncin, J.-Y., and Damany, H. (1970). Fundamental absorption spectrum of solid neon. *Phys. Rev. Lett.* 25, 1279–1280. doi:10.1103/PhysRevLett.25.1279

Bukow, H. H., Heine, G., and Reinke, M. (1977). Lifetime measurements of atomic states of He I. *J. Phys. B Atomic Mol. Phys.* 10, 2347–2358. doi:10.1088/0022-3700/10/12/013

Calvani, P., De Simone, C., Giovannelli, A. B., and Maraviglia, B. (1974). Neutral excitations in liquid Helium. *Nuovo Cim. B* 19, 271–287. doi:10.1007/BF02895649

Cao, H., Alexander, T., Aprahamian, A., Avetisyan, R., Back, O., Cocco, G., et al. (2015). Measurement of scintillation and ionization yield and scintillation pulse shape from nuclear recoils in liquid argon. *Phys. Rev. D.* 91, 092007. doi:10.1103/physrevd.91.092007

Danylchenko, O. G., Boltnev, R. E., Khmelenko, V. V., Kiryukhin, V., Konotop, O. P., Lee, D. M., et al. (2017). Argon nanoclusters with fivefold symmetry in supersonic gas jets and superfluid helium. *J. Low. Temp. Phys.* 187, 156–165. doi:10.1007/s10909-016-1720-8

Danylchenko, O. G., Doronin, Y. S., Kovalenko, S. I., and Samovarov, V. N. (2006). Phase separation into pure components in mixed Ar-Xe clusters. *JETP Lett.* 84, 324–328. doi:10.1134/S002136400618010X

Dennis, W. S., Durbin, E. J. R., Fitzsimmons, W. A., Heybey, O., and Walters, G. K. (1969). Spectroscopic identification of excited atomic and molecular states in electron-bombarded liquid helium. *Phys. Rev. Lett.* 23, 1083–1086. doi:10.1103/PhysRevLett.23.1083

Donnelly, R. J., and Barenghi, C. F. (1998). The observed properties of liquid helium at the saturated vapor pressure. *J. Phys. Chem. Reference Data* 27, 1217–1274. doi:10.1063/1.556028

Efimov, V. B., Mezhov-Deglin, L. P., Dewhurst, C. D., Lokhov, A. V., and Nesvizhevsky, V. V. (2015). Neutron scattering on impurity nanoclusters in gel samples. *Adv. High Energy Phys.* 2015, 1–4. doi:10.1155/2015/808212

Ehler, A. W., and Weissler, G. L. (1955). Ultraviolet absorption of atomic nitrogen in its ionization continuum. *J. Opt. Soc. Am.* 45, 1035–1043. doi:10.1364/josa.45.001035

Feng, J. L. (2010). Dark matter candidates from particle physics and methods of detection. *Annu. Rev. Astron Astrophys.* 48, 495–545. doi:10.1146/annurev-astro-082708-101659

Fonda, E., Sreenivasan, K. R., and Lathrop, D. P. (2016). Sub-micron solid air tracers for quantum vortices and liquid helium flows. *Rev. Sci. Instrum.* 87, 025106. doi:10.1063/1.4941337

Fowler, W. B., and Dexter, D. L. (1968). Electronic bubble states in liquid helium. *Phys. Rev.* 176, 337–343. doi:10.1103/PhysRev.176.337

Francini, R., Montereali, R. M., Nichelatti, E., Vincenti, M. A., Canci, N., Segreto, E., et al. (2013). VUV-Vis optical characterization of Tetraphenyl-butadiene films on glass and specular reflector substrates from room to liquid Argon temperature. *J. Instrum.* 8, P09006. doi:10.1088/1748-0221/8/09/p09006

Fugol', I. Y. A., Savchenko, E. V., and Belov, A. G. (1972). Luminescence of solid neon. *Sov. JETP Lett.* 16, 172–174.

Gabal, M., Sese, J., Rillo, C., and Spagna, S. (2018). ""Clean" liquid helium," in *Superfluids and superconductors*. Editor R. Zivieri (London: IntechOpen), 67–86. doi:10.5772/intechopen.74907

Ghosh, A., and Maris, H. J. (2005). Observation of a new type of electron bubble in superfluid helium. *Phys. Rev. Lett.* 95, 265301. doi:10.1103/physrevlett.95.265301

Golov, A., and Ishimoto, H. (1998). Sharp and stable metal tips for helium ionization at mK temperatures. *J. Low Temp. Phys.* 113, 957–962. doi:10.1023/A:1022583729253

Gordon, E. B., Karabulin, A. V., Matyushenko, V. I., Sizov, V. D., and Khodos, I. I. (2012). The role of vortices in the process of impurity nanoparticles coalescence in liquid helium. *Chem. Phys. Lett.* 519–520, 64–68. doi:10.1016/j.cplett.2011.11.020

Gordon, E. B., Khmelenko, V. V., Pelmenev, A. A., Popov, E. A., Pugachev, O. F., and Shestakov, A. F. (1993). Metastable impurity-helium solid phase. Experimental and theoretical evidence. *Chem. Phys.* 170, 411–426. doi:10.1016/0301-0104(93)85122-O

Gordon, E. B., Mezhov-Deglin, L. P., and Pugachev, O. F. (1974). Stabilization of nitrogen atoms in superfluid helium. *JETP Lett.* 19, 63–65.

Gordon, E. B., Pelmenev, A. A., Pugachev, O. F., and Khmelenko, V. V. (1983). Hydrogen and deuterium atoms, stabilized by condensation of an atomic beam in superfluid helium. *JETP Lett.* 37, 282–285.

Gu, F., Zhou, J., Liao, J., Gao, Y., Liang, Z., Ma, M., et al. (2024). A novel nuclear recoil calibration for liquid helium detectors. *Eur. Phys. J. Plus* 139, 437. doi:10.1140/epjp/s13360-024-05195-y

Guo, W., Dufault, M., Cahn, S. B., Nikkel, J. A., Shin, Y., and McKinsey, D. N. (2012). Scintillation and charge yield from the tracks of energetic electrons in superfluid helium-4. *J. Instrum.* 7, P01002. doi:10.1088/1748-0221/7/01/P01002

Guo, W., and McKinsey, D. N. (2013). Concept for a dark matter detector using liquid helium-4. *Phys. Rev. D.* 87, 115001. doi:10.1103/PhysRevD.87.115001

Gürtler, P., Saile, V., and Koch, E. E. (1977). High resolution absorption spectrum of nitrogen in the vacuum ultraviolet. *Chem. Phys. Lett.* 48, 245–250. doi:10.1016/0009-2614(77)80308-4

Haensel, R., Koch, E. E., Kosuch, N., Nielsen, U., and Skibowski, M. (1971). Vacuum ultraviolet reflectivity of solid nitrogen and oxygen. *Chem. Phys. Lett.* 9, 548–550. doi:10.1016/0009-2614(71)85122-9

Harrison, M. K., Lippincott, W. H., McKinsey, D. N., and Nikkel, J. A. (2007). Use of activated charcoal for the purification of neon in the CLEAN experiment. *Nucl. Instrum. Methods Phys. Res. Sect. A Accel. Spectrom. Detect. Assoc. Equip.* 570, 556–560. doi:10.1016/j.nima.2006.10.135

Hertel, S., Biekert, A., Lin, J., Velan, V., and McKinsey, D. (2019). Direct detection of sub-Gev dark matter using a superfluid ^{4}He target. *Phys. Rev. D.* 100, 092007. doi:10.1103/PhysRevD.100.092007

Herzfeld, C. M., and Broida, H. P. (1956). Interpretation of spectra of atoms and molecules in solid nitrogen condensed at 4.2°K. *Phys. Rev.* 101, 606–611. doi:10.1103/PhysRev.101.606

Hill, P. C. (1989). Ultraviolet continua of helium molecules. *Phys. Rev. A* 40, 5006–5016. doi:10.1103/PhysRevA.40.5006

Huber, K. P., and Herzberg, G. (1979). *Molecular spectra and molecular structure. IV. Constants of diatomic molecules*. New York: Van Nostrand.

Ito, T. M., Clayton, S. M., Ramsey, J., Karcz, M., Liu, C.-Y., Long, J. C., et al. (2012). Effect of an electric field on superfluid helium scintillation produced byα-particle sources. *Phys. Rev. A* 85, 042718. doi:10.1103/physreva.85.042718

Ito, T. M., and Seidel, G. M. (2013). Scintillation of liquid helium for low-energy nuclear recoils. *Phys. Rev. C* 88, 025805. doi:10.1103/physrevc.88.025805

Jesse, W. P., and Sadauskis, J. (1955). Ionization in pure gases and the average energy to make an ion pair for alpha and beta particles. *Phys. Rev.* 97, 1668–1670. doi:10.1103/physrev.97.1668

Jewell, C., and McClintock, P. V. E. (1979). A note on the purity of liquid helium-4. *Cryogenics* 19, 682–683. doi:10.1016/0011-2275(79)90073-0

Jortner, J., Meyer, L., Rice, S. A., and Wilson, E. G. (1964). Energy transfer phenomena in liquid helium. *Phys. Rev. Lett.* 12, 415–416. doi:10.1103/PhysRevLett.12.415

Kahn, Y., and Lin, T. (2022). Searches for light dark matter using condensed matter systems. *Rep. Prog. Phys.* 85, 066901. doi:10.1088/1361-6633/ac5f63

Kempter, V., Veith, F., and Zehnle, L. (1975). Excitation processes in low-energy collisions between ground state helium atoms. *J. Phys. B Atomic Mol. Phys.* 8, 1041–1051. doi:10.1088/0022-3700/8/7/010

Keto, J. W., Soley, F. J., Stockton, M., and Fitzsimmons, W. A. (1974). Dynamic properties of neutral excitations produced in electron-bombarded superfluid helium. II. Afterglow fluorescence of excited helium molecules. *Phys. Rev. A* 10, 887–896. doi:10.1103/physreva.10.887

Khmelenko, V. V., Lee, D. M., Krushinskaya, I. N., Boltnev, R. E., Bykhalo, I. B., and Pelmenev, A. A. (2012). Dynamics of thermoluminescence spectra of impurity-helium condensates containing stabilized nitrogen and oxygen atoms. *Low. Temp. Phys.* 38, 688–699. doi:10.1063/1.4745675

Kiryukhin, V., Bernard, E. P., Khmelenko, V. V., Boltnev, R. E., Krainyukova, N. V., and Lee, D. M. (2007). Noble gas nanoclusters with five-fold symmetry stabilized in superfluid helium. *Phys. Rev. Lett.* 98, 195506. doi:10.1103/PhysRevLett.98.195506

Kiryukhin, V., Keimer, B., Boltnev, R. E., Khmelenko, V. V., and Gordon, E. B. (1997). Inert-gas solids with nanoscale porosity. *Phys. Rev. Lett.* 79, 1774–1777. doi:10.1103/PhysRevLett.79.1774

Kiselev, S. I., Khmelenko, V. V., and Lee, D. M. (2002). Hydrogen atoms in impurity-helium solids. *Phys. Rev. Lett.* 89, 175301. doi:10.1103/PhysRevLett.89.175301

Kiselev, S. I., Khmelenko, V. V., Lee, D. M., Kiryukhin, V., Boltnev, R. E., Gordon, E. B., et al. (2001). Structural studies of impurity-helium solids. *Phys. Rev. B* 65, 024517. doi:10.1103/PhysRevB.65.024517

Kondev, F. G., Wang, M., Huang, W. J., Naimi, S., and Audi, G. (2021). The NUBASE2020 evaluation of nuclear physics properties *. *Chin. Phys. C* 45, 030001. doi:10.1088/1674-1137/abddae

Krainyukova, N. V., Boltnev, R. E., Bernard, E. P., Khmelenko, V. V., Lee, D. M., and Kiryukhin, V. (2012). Observation of the fcc-to-hcp transition in ensembles of argon nanoclusters. *Phys. Rev. Lett.* 109, 245505. doi:10.1103/PhysRevLett.109.245505

Kunsch, P. L., and Dressler, K. (1978). Calculation of dynamically induced electronic transitions of matrix-isolated atomic nitrogen. *J. Chem. Phys.* 68, 2550–2561. doi:10.1063/1.436114

Laasch, W., Hagedorn, H., Kloiber, T., and Zimmerer, G. (1990). Fine structure of the luminescence of solid neon and its relation to exciton trapping and desorption induced by excitonic excitation. *Phys. status solidi (b)* 158, 753–767. doi:10.1002/pssb.2221580236

Li, Z.-L., Bonifaci, N., Aitken, F., Denat, A., von Haeften, K., Atrazhev, V. M., et al. (2009). Spectroscopic investigation of liquid helium excited by a corona discharge: evidence for bubbles and red satellites. *Eur. Phys. J. Appl. Phys.* 47, 22821. doi:10.1051/epjap/2009092

Liao, J., Gao, Y., An, G., Gu, F., Hu, S., Liang, Z., et al. (2023b). Search for ER and/or NR-like dark matter signals with the especially low background liquid helium TPCs. arXiv:2302.12406v4

Liao, J., Gao, Y., Liang, Z., Ouyang, Z., Peng, Z., Zhang, L., et al. (2022). Introduction to a low-mass dark matter project, ALETHEIA: a Liquid hElium Time projection cHambEr in dArk matter. arXiv:2203.

Liao, J., Gao, Y., Liang, Z., Ouyang, Z., Peng, Z., Zhang, L., et al. (2023a). Aletheia: hunting for low-mass dark matter with liquid helium TPCs. *Eur. Phys. J. Plus* 138, 128. doi:10.1140/epjp/s13360-023-03747-2

Lin, T. (2019). Dark matter models and direct detection. *Proc. Theor. Adv. Study Inst. Summer Sch. 2018 Theory Era Data — PoS(TASI2018)* 333, 009. doi:10.22323/1.333.0009

Loveland, R. J., Le Comber, P. G., and Spear, W. E. (1972). Experimental evidence for electronic bubble states in liquid Ne. *Phys. Lett. A* 39, 225–226. doi:10.1016/0375-9601(72)90717-7

Maris, H. J., Seidel, G. M., and Stein, D. (2017). Dark matter detection using helium evaporation and field ionization. *Phys. Rev. Lett.* 119, 181303. doi:10.1103/PhysRevLett.119.181303

McColgan, P. T., Meraki, A., Boltnev, R. E., Lee, D. M., and Khmelenko, V. V. (2017a). Luminescence of molecular nitrogen nanoclusters containing stabilized atoms. *J. Phys. Chem. A* 121, 9045–9057. doi:10.1021/acs.jpca.7b09661

McColgan, P. T., Meraki, A., Boltnev, R. E., Lee, D. M., and Khmelenko, V. V. (2017b). Optical and electron spin resonance studies of destruction of porous structures formed by nitrogen-rare gas nanoclusters in bulk superfluid helium. *J. Low. Temp. Phys.* 187, 124–139. doi:10.1007/s10909-016-1707-5

McColgan, P. T., Sheludiakov, S., Rentzepis, P. M., Lee, D. M., and Khmelenko, V. V. (2019). Rotationally induced luminescence of nanoclusters immersed in superfluid helium. *Low. Temp. Phys.* 45, 310–316. doi:10.1063/1.5090088

McKinsey, D. N., Brome, C. R., Butterworth, J. S., Dzhosyuk, S. N., Huffman, P. R., Mattoni, C. E. H., et al. (1999). Radiative decay of the metastable $He_2(a^3\Sigma_u^+)$ molecule in liquid helium. *Phys. Rev. A* 59, 200–204. doi:10.1103/PhysRevA.59.200

McKinsey, D. N., Brome, C. R., Dzhosyuk, S. N., Golub, R., Habicht, K., Huffman, P. R., et al. (2003). Time dependence of liquid-helium fluorescence. *Phys. Rev. A* 67, 062716. doi:10.1103/PhysRevA.67.062716

McKinsey, D. N., and Doyle, J. M. (2000). Liquid helium and liquid neon-sensitive, low background scintillation media for the detection of low energy neutrinos. *J. Low Temp. Phys.* 118, 153–165. doi:10.1023/A:1004690906370

Mehrotra, R., Mann, E. K., and Dahm, A. J. (1979). A study of the neutral excitation current in liquid ^{4}He above 1 K. *J. Low. Temp. Phys.* 36, 47–65. doi:10.1007/BF00174911

Meraki, A., Mao, S., McColgan, P. T., Boltnev, R. E., Lee, D. M., and Khmelenko, V. V. (2016). Thermoluminescence dynamics during destructions of porous structures formed by nitrogen nanoclusters in bulk superfluid helium. *J. Low. Temp. Phys.* 185, 269–286. doi:10.1007/s10909-016-1557-1

Meraki, A., McColgan, P. T., Boltnev, R. E., Lee, D. M., and Khmelenko, V. V. (2018). Electron spin resonance studies of nitrogen atoms stabilized in impurity-helium condensates. *J. Low. Temp. Phys.* 192, 224–240. doi:10.1007/s10909-018-1952-x

Meraki, A., McColgan, P. T., Rentzepis, P. M., Li, R. Z., Lee, D. M., and Khmelenko, V. V. (2017). Quantum vortices and thermally induced luminescence of nitrogen nanoclusters immersed in liquid helium. *Phys. Rev. B* 95, 104502. doi:10.1103/PhysRevB.95.104502

Mezhov-Deglin, L. P., Efimov, V. B., Lokhov, A. V., Lychagin, E. V., Muzychko, A. Y., Nesvizhevskii, V. V., et al. (2007). Scattering of cold neutrons on gel samples formed by impurity clusters in superfluid He-ii. *J. Low. Temp. Phys.* 148, 833–837. doi:10.1007/s10909-007-9460-4

Michniak, R. A., Alleaume, R., McKinsey, D. N., and Doyle, J. M. (2002). Alpha and beta particle induced scintillations in liquid and solid neon. *Nucl. Instrum. Methods Phys. Res. Sect. A Accel. Spectrom. Detect. Assoc. Equip.* 482, 387–394. doi:10.1016/S0168-9002(01)01503-0

Moon, C. J., Erukala, S., Feinberg, A. J., Singh, A., Choi, M. Y., and Vilesov, A. F. (2023). Formation of the $C_4H_n^+$ (n = 2-5) ions upon ionization of acetylene clusters in helium droplets. *J. Chem. Phys.* 158, 224307. doi:10.1063/5.0150700

Moroshkin, P., Hofer, A., and Weis, A. (2008). Atomic and molecular defects in solid ^{4}He. *Phys. Rep.* 469, 1–57. doi:10.1016/j.physrep.2008.06.004

Moroshkin, P., Lebedev, V., and Weis, A. (2011). Phonon generation in condensed ^{4}He by laser-excited atomic bubbles. *EPL Europhys. Lett.* 96, 26002. doi:10.1209/0295-5075/96/26002

Nakai, H., Kimura, N., Murakami, M., Haruyama, T., and Yamamoto, A. (1996). Superfluid helium flow through porous media. *Cryogenics* 36, 667–673. doi:10.1016/0011-2275(96)00030-6

Neeser, S., Tietz, R., Schulz, M., and Langhoff, H. (1994). Lifetime of the He_2(e), He_2(d) and He_2(f) states. *Zeitschrift für Physik D Atoms, Mol. Clust.* 31, 61–65. doi:10.1007/BF01426580

Oehler, O., Smith, D. A., and Dressler, K. (1977). Luminescence spectra of solid nitrogen excited by electron impact. *J. Chem. Phys.* 66, 2097–2107. doi:10.1063/1.434171

O'Hare, C. A. J. (2021). New definition of the neutrino floor for direct dark matter searches. *Phys. Rev. Lett.* 127, 251802. doi:10.1103/PhysRevLett.127.251802

Peng, Z., Zhongjun, H., Bingming, W., and Qing, L. (2018). Design of a nitrogen purification system with cryogenic method for neutrino detection. *Appl. Radiat. Isotopes* 137, 194–198. doi:10.1016/j.apradiso.2018.04.009

Peyron, M., and Broida, H. P. (1959). Spectra emitted from solid nitrogen condensed at very low temperatures from a gas discharge. *J. Chem. Phys.* 30, 139–150. doi:10.1063/1.1729865

Popov, E., Ahokas, J., Eloranta, J., and Kunttu, H. (2005). Generation of intrinsic excitations in superfluid ^{4}He by using gas jet approach. *J. Low. Temp. Phys.* 138, 85–90. doi:10.1007/s10909-005-1532-8

Rayfield, G. W., and Reif, F. (1964). Quantized vortex rings in superfluid helium. *Phys. Rev.* 136, A1194–A1208. doi:10.1103/physrev.136.a1194

Reif, F., and Meyer, L. (1960). Study of superfluidity in liquid He by ion motion. *Phys. Rev.* 119, 1164–1173. doi:10.1103/physrev.119.1164

Ruchti, T., Förde, K., Callicoatt, B. E., Ludwigs, H., and Janda, K. C. (1998). Charge transfer and fragmentation of liquid helium clusters that contain one or more neon atoms. *J. Chem. Phys.* 109, 10679–10687. doi:10.1063/1.477765

Santos, D., Mayet, F., Guillaudin, O., Lamy, T., Ranchon, S., Trichet, A., et al. Ionization quenching factor measurement of helium 4. (2008). arXiv:0810.1137

Sato, S., Kowari, K., and Okazaki, K. (1976). A comparison of the primary processes of the radiolyses induced by α-β-and γ-rays. *Bull. Chem. Soc. Jpn.* 49, 933–936. doi:10.1246/bcsj.49.933

Savchenko, E., Khyzhniy, I., and Bondybey, V. (2019). New trends in spectroscopy of solid nitrogen. *Low. Temp. Phys.* 45, 975–987. doi:10.1063/1.5121267

Savchenko, E. V., Khyzhniy, I. V., Uyutnov, S. A., Barabashov, A. P., Gumenchuk, G. B., Beyer, M. K., et al. (2015). Radiation effects in solid nitrogen and nitrogen-containing matrices: fingerprints of N_4^+ species. *J. Phys. Chem. A* 119, 2475–2482. doi:10.1021/jp5087575

Sayer, R. J., Prince, R. H., and Duley, W. W. (1981). Emission spectra of O and N atoms and the structure of solid N_2/Ne mixtures. *Phys. status solidi (b)* 106, 249–258. doi:10.1002/pssb.2221060128

Schuberth, E., and Creuzburg, M. (1975). X-Ray-Induced vacuum ultraviolet luminescence from neon crystals. *Phys. status solidi (b)* 71, 797–802. doi:10.1002/pssb.2220710243

Scott, T. A. (1976). Solid and liquid nitrogen. *Phys. Rep.* 27, 89–157. doi:10.1016/0370-1573(76)90032-6

Sethumadhavan, B. (2007). *Charge Gain and Breakdown in Liquid Helium at Low Temperatures*. [PhD dissertation]. Providence, RI: Brown University.

Smirnov, B. M. (2018). *Physics of atoms and ions*. Cham: Springer, 219. doi:10.1007/978-3-319-75405-5_3

Sommer, W. T. (1964). Liquid helium as a barrier to electrons. *Phys. Rev. Lett.* 12, 271–273. doi:10.1103/PhysRevLett.12.271

Song, K. S., and Williams, R. T. (1996). *Self-trapped excitons*. 2-nd edition. Berlin, Heidelberg: Springer, 410. doi:10.1007/978-3-642-85236-7

Stockton, M., Keto, J. W., and Fitzsimmons, W. A. (1972). Ultraviolet emission spectrum of electron-bombarded superfluid helium. *Phys. Rev. A* 5 (5), 372–380. doi:10.1103/PhysRevA.5.372

Storchak, V. G., Eshchenko, D. G., Brewer, J. H., Cottrell, S. P., Cox, S. F. J., Karlsson, E., et al. (2001). Electron transport in cryocrystals. *J. Low Temp. Phys.* 122, 527–535. doi:10.1023/a:1004842026921

Sullivan, I. S., Niemela, J. J., Hershberger, R. E., Bolster, D., and Donnelly, R. J. (2008). Dynamics of thin vortex rings. *J. Fluid Mech.* 609, 319–347. doi:10.1017/S0022112008002292

Surko, C. M., Packard, R. E., Dick, G. J., and Reif, F. (1970). Spectroscopic study of the luminescence of liquid helium in the vacuum ultraviolet. *Phys. Rev. Lett.* 24, 657–659. doi:10.1103/physrevlett.24.657

Talman, J. D., and Frolov, A. M. (2006). Excitations of light atoms during nuclear reactions with fast neutrons. *Phys. Rev. A* 73, 032722. doi:10.1103/PhysRevA.73.032722

Tinti, D. S., and Robinson, G. W. (1968). Spectroscopic evidence for slow vibrational and electronic relaxation in solids. The vegard–kaplan and second positive systems of N_2 in solid rare gases. *J. Chem. Phys.* 49, 3229–3245. doi:10.1063/1.1670575

Torquato, S., and Lu, B. (1993). Chord-length distribution function for two-phase random media. *Phys. Rev. E* 47, 2950–2953. doi:10.1103/physreve.47.2950

Toschi, F., Brunold, A., Burmeister, L., Eitel, K., Enss, C., Fascione, E., et al. (2025). Signal partitioning in superfluid ^{4}He: a Monte Carlo approach. *Phys. Rev. D.* 111, 032013. doi:10.1103/PhysRevD.111.032013

Trickl, T., Cromwell, E. F., Lee, Y. T., and Kung, A. H. (1989). *State-selective ionization of nitrogen in the X_2 v=0 and v=1 states by two-color (1+1) photon excitation near threshold. J. Chem. Phys.* 91, 6006–6012. doi:10.1063/1.457417

Trottier, A., Jirasek, A. I., Tiedje, H. F., and Brooks, R. L. (2000). Spectra of liquid helium and hydrogen-doped liquid helium. *Phys. Rev. A* 61, 052504. doi:10.1103/physreva.61.052504

von Krosigk, B., Eitel, K., Enss, C., Ferber, T., Gastaldo, L., Kahlhoefer, F., et al. (2023). DELight: a Direct search Experiment for Light dark matter with superfluid helium. *Sci. Post. Phys. Proc.* 12, 016. doi:10.21468/SciPostPhysProc.12.016

Wetzel, C. K., Lee, D. M., and Khmelenko, V. V. (2024a). Structure of molecular nitrogen nanoclusters containing stabilized nitrogen atoms. *J. Low. Temp. Phys.* 220, 25–40. doi:10.1007/s10909-024-03225-8

Wetzel, C. K., Lee, D. M., and Khmelenko, V. V. (2024b). Studies of the structures of nitrogen-neon nanoclusters immersed into superfluid helium-4. *J. Low. Temp. Phys.* 215, 294–311. doi:10.1007/s10909-023-03026-5

Wieser, M. E., and Coplen, T. B. (2010). Atomic weights of the elements 2009 (IUPAC technical report). *Pure Appl. Chem.* 83, 359–396. doi:10.1351/PAC-REP-10-09-14

You, Y., Smolinsky, J., Xue, W., Matchev, K., Saab, T., Gunther, K., et al. (2023). Signatures and detection prospects for sub-GeV dark matter with superfluid helium. *J. High Energy Phys.* 2023, 9. doi:10.1007/JHEP07(2023)009